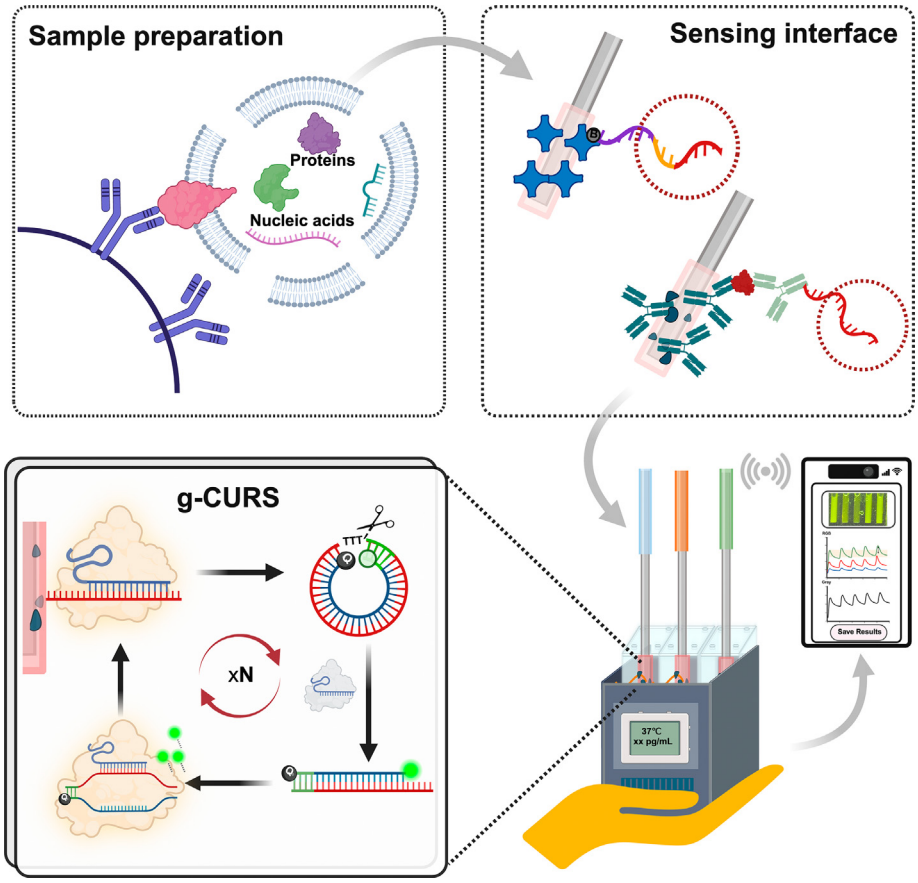
Trends in Biotechnology

CellPress

Research Article

Glass fiber-interfaced CRISPR/Cas biosensing adaptable for diverse biomarker detection



A glass-fiber interfaced CRISPR/Cas biosensor introduces a universal reagent setting for multiplex detection of nucleic acids and proteins with exceptional sensitivity through cascade amplification. Compatible with portable fluorescence readers, this system delivers rapid results from only 5-μl samples, making it an ideal solution for point-of-care diagnostics and personalized medicine

Tian Yu, Siyi Zou, Yingxi Long, Yourong Ou, Shixian Liu, Tongjia Kang, Libing Song, Congcong Sun, Guozhen Liu

liuguozhen@cuhk.edu.cn (G. Liu).

Highlights

The glass fiber interfaced CRISPR/Cas with a universal reagent setting (g-CURS) system was developed to simplify and standardize CRISPR/Cas biosensing, enabling simultaneous detection of diverse analytes while eliminating the need for CRISPR RNA (crRNA) and single-stranded DNA (ssDNA) activator screening.

The g-CURS system demonstrated the ability to discriminate point mutations using ligase-based target recognition strategies in nucleic acid detection.

CRISPR/Cas12a-assisted rapid and exponential cascade amplification was achieved using circular reporters (CRs), enabling ultra-high specificity and sensitivity suitable for detecting trace analytes.

With the aid of a portable fluorescence reader, the g-CURS system enabled rapid detection of multiple nucleic acids within 30 min and multiple proteins within 80 min using a minimal sample volume of only 5 μl, making it highly suitable for point-of-care testing.

Trends in Biotechnology, August 2025, Vol. 43, No. 8
https://doi.org/10.1016/j.tibtech.2025.05.001

© 2025 Elsevier Ltd. All rights are reserved, including those for text and data mining, AI training, and similar technologies.

CellPress

Trends in Biotechnology

Research Article

Glass fiber-interfaced CRISPR/Cas biosensing adaptable for diverse biomarker detection

Tian Yu[1], Siyi Zou[1], Yingxi Long[1], Yourong Ou[1], Shixian Liu[1], Tongjia Kang[1], Libing Song[2], Congcong Sun[3], and Guozhen Liu [1,4,*]

Developing a generic sensitive platform for detecting diverse biomarkers is essential for a comprehensive understanding of disease states, guiding precision medicine. Herein, we introduce a versatile platform based on glass fiber interfaced CRISPR/Cas with a universal reagent setting (g-CURS), which used a fixed pair of CRISPR RNA (crRNA) and a single-stranded DNA (ssDNA) activator to enable detection of multiple nucleic acids or proteins with ultrahigh sensitivity. The fixed ssDNA activator was labeled on multiple specific ligation products or detection antibodies conjugated on glass fiber to initiate CRISPR/Cas12a-assisted rapid and exponential cascade amplification through circular reporters (CRs), generating fluorescence signals readable by a portable detector. g-CURS was able to detect viral nucleic acids with attomolar sensitivity within 30 min and multiple low-abundance proteins in extracellular vesicles of Parkinson's disease (PD) serum with subpicomolar sensitivity within 80 min. g-CURS simplifies CRISPR/Cas biosensing using a standard reagent setting, holding promise for biomarker discovery free from bulky instruments.

Technology readiness

The glass-fiber interfaced CRISPR/Cas with a universal reagent setting (g-CURS) system introduced in this study is currently at Technology Readiness Level (TRL) 4, signifying its validation in laboratory settings using representative clinical samples. g-CURS has been demonstrated to be a versatile platform that uses a fixed pair of CRISPR RNA (crRNA) and single-stranded (ss)DNA activators for multiplex detection of nucleic acids and proteins, achieving attomolar sensitivity for nucleic acid detection within 30 min, and subpicomolar sensitivity for multiple proteins within 80 min. However, several challenges must be addressed before full implementation. Notably, efficient and convenient sample pretreatment methods capable of extracting both nucleic acids and proteins within a simple setup are crucial for improving detection accuracy and minimizing sample consumption, thereby making the system more suitable for point-of-care testing.

Introduction

Ultrasensitive quantification of diverse biomarkers in body fluids is crucial for a comprehensive understanding of disease development and progression and to subsequently guide precision medicine [1]. Developing generic technologies that enable rapid and sensitive detection of various biomolecules (such as nucleic acids and proteins) is increasingly in demand for accurate assessment of the states of infectious diseases [2,3] and also for enhancing the precision of the prognosis, diagnosis, and treatment of chronic diseases [4–8]. For example, the microfluidic electrochemical sensor developed by Najjar and coworkers [9] enhanced the monitoring of the distinct clinical timelines of severe acute respiratory syndrome-coronavirus 2 (SARS-CoV-2) infections, characterized by viral RNA and IgG antibodies, although the assay involved an intricated primer design for each analyte. Similarly, a high-throughput nano-biochip integrated system for liquid biopsy analysis [10] allowed the detection of proteins and mRNA/miRNA at a single vesicle level, providing comprehensive information on extracellular vesicle (EV) phenotypes and disease states. However, it heavily relied on expensive total internal reflective fluorescence microscopy. In addition, a cost-effective multianalyte lateral flow immunoassay [11] was used to detect bacterial DNA and host inflammatory biomarkers, but had a protein detection limit of 4 ng/ml, which was not sufficient for detecting low-abundance proteins, such as those secreted by a single tumor cell into the bloodstream or the *p24* capsid antigen in serum from individuals recently infected with HIV [12,13]. Thus, to address practical applications, a single assay capable of detecting diverse analytes must be further enhanced in terms of sensitivity, assay time, simplicity, portability, and other key aspects.

Beyond the well-known capability of gene editing, the CRISPR system, with its high programmability and rapidly specific target recognition [14], has been applied extensively in intracellular

[1]Integrated Devices and Intelligent Diagnosis (ID[2]) Laboratory, CUHK(SZ)-Boyalife Joint Laboratory of Regenerative Medicine Engineering, School of Medicine, The Chinese University of Hong Kong, Shenzhen, 518172, China
[2]Department of Experimental Research, Sun Yat-sen University Cancer Center, State Key Laboratory of Oncology in South China, Collaborative Innovation Center for Cancer Medicine, Guangzhou, 510060, China
[3]Department of Neurology, Qilu Hospital of Shandong University, Jinan, Shandong Province, 250012, China
[4]Website: www.x-mol.com/groups/liu_guozhen?lang=en

*Correspondence: liuguozhen@cuhk.edu.cn (G. Liu).

© 2025 Elsevier Ltd. All rights reserved, including those for text and data mining, AI training, and similar technologies.

imaging, biosensing, point-of-care (POC) diagnosis [15], and other fields [16]. Its outstanding dual features of recognition and transduction enable programmable CRISPR/Cas systems to be integrated with various biosensing systems [15], with superiority in detecting diverse analytes from nucleic acids to proteins and small molecules, and so on [17]. However, CRISPR/Cas-assisted nucleic acid biosensing technologies often require the development of specific reagents for each analyte, where unique crRNAs and ssDNA activators are tailored for each target gene. Limitations to the specificity of ssDNA activators or the need for accessible protospacer-adjacent motif (PAM) sites in target DNA when using double-stranded DNA (dsDNA) activators [18] complicate the selection of detection sites in nucleic acid assays and the screening of corresponding crRNAs. In addition, CRISPR/Cas biosensors based on the trans-cleavage enzymatic activity of Class2 V and VI Cas nucleases unavoidably encounter challenges of inadequate sensitivity (at approximately the picomolar level) [19,20]. To address the knowledge gap, it is essential to develop a generic detection platform integrated with the CRISPR/Cas system to realize the simultaneous ultrasensitive detection of diverse analytes under standardized conditions, especially at POC.

In this study, we developed g-CURS, which can detect multiple nucleic acids and proteins with a fixed set of crRNA and ssDNA activators (Figure 1). To enable the detection of various types of

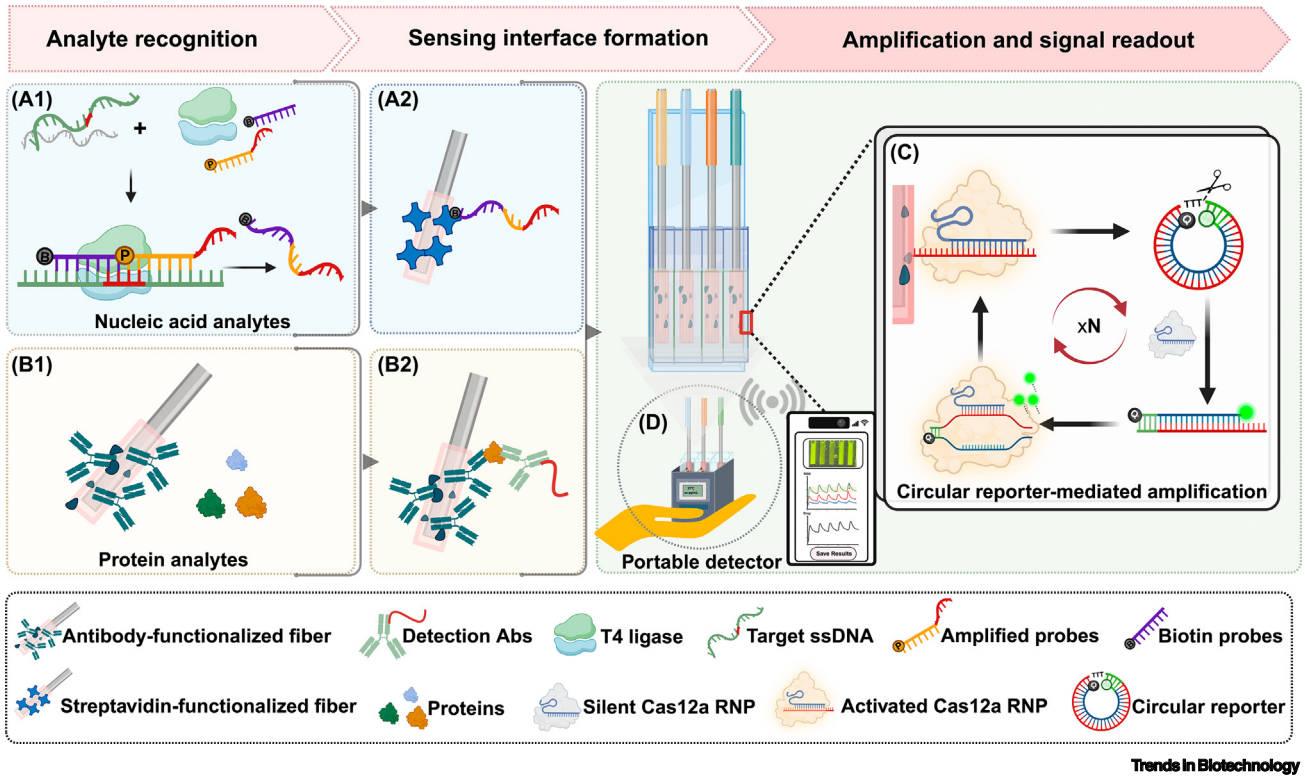


Figure 1. Workflow of glass-fiber interfaced CRISPR/Cas with a universal reagent setting (g-CURS) for ultrasensitive detection of nucleic acids and proteins. Different functionalized glass fibers were used to capture nucleic acids and proteins. (Ai) T4 ligase-mediated nucleic acid target recognition. (ii) Ligation products can be captured and purified through biotin–streptavidin (SA) interactions on functionalized glass fibers after completing target recognition. (Bi) Modification of capture antibodies (Abs) on a glass fiber to capture protein analytes. (ii) Formation of a sandwich immunoassay on a glass fiber. (C) Designed target sequence recognition process facilitated by T4 ligase and the single-stranded (ss)DNA activator-conjugated detection antibody enables multitarget detection using a pair of fixed ssDNA activators and matching CRISPR (cr)RNA based on circular reporter (CR)-mediated-CRISPR/Cas biosensing to generate an exponential fluorescence signal. (D) Quantification of the generated fluorescent signal by the homemade portable detector. Figure created with BioRender (biorender.com); for image licenses, please refer to the supplemental information online. Abbreviation: RNP, ribonucleoprotein.

low-abundant analyte with reduced assay times while preserving high sensitivity, g-CURS eliminates traditional preamplification strategies [21–24] in CRISPR/Cas biosensing systems, such as recombinase polymerase amplification (RPA) [25,26], loop-mediated isothermal amplification (LAMP) [27], and rolling circle amplification (RCA) [28]. g-CURS uses a preamplification-free strategy based on cascade amplification techniques, as used in the CRISPR/Cas-only amplification network (CONAN) [29] and the Autocatalytic Cas12a Circular DNA Amplification Reaction (AutoCAR) system using a CR [30]. In addition, to address the limited specificity of the ssDNA activator and to simplify the complexity of detection-site selection and the corresponding crRNA screening, g-CURS-assisted nucleic acid detection took advantage of the ability of T4 DNA ligase to join two adjacent and perfectly matched target DNA oligonucleotides on complementary DNA templates (the cDNA reverse-transcribed from an mRNA template or a ssDNA target) (Figure 1Ai), with the ability to recognize single-base mismatches [31–34]. Simultaneously, to enable the detection of multiple proteins, g-CURS was integrated with an immunoassay comprising a specific capture antibody immobilized on a glass fiber (Figure 1Bi) and an ssDNA activator-labeled detection antibody (dAb) for detecting each target protein. After the dual purification effects of high salt ions and formamide (wash buffer F), ligated DNA products are effectively captured by the streptavidin (SA)-modified solid phase. Thus, the ssDNA activator labeled on the newly ligated DNA products (Figure 1Aii) or on detection antibodies (Figure 1Bii) can form individual sensing interfaces on a specific glass fiber. These interfaces trigger subsequent CR-mediated CRISPR/Cas cascade amplification reactions (Figure 1C), converting target DNA or protein information into corresponding fluorescent signals. Finally, the g-CURS-assisted nucleic acid and protein detection system was integrated with a previously reported portable detection platform [35] to achieve the large instrument-free detection of multiple types of analyte in a POC setting (Figure 1D).

In our experiments, CR-mediated CRISPR/Cas cascade amplification significantly enhanced the detection limit by four to five orders of magnitude under isothermal reaction conditions (from the picomolar to the attomolar range) within 30 min, compared with linear reporter (LR)-based CRISPR/Cas12a biosensing methods in homogeneous solutions. Variants of SARS-COV-2, which acquires increasingly contagious mutations as it evolves [36,37] and of high-risk human papillomavirus (hrHPV) were used as model analytes of infectious diseases. Using Delta spike protein cDNA and HPV16 E7 cDNA as examples, g-CURS achieved a subfemtomolar detection limit with a 10-min ligation and a 15-min CR-assisted amplification. The system was further validated using 56 HPV16 clinical samples, demonstrating 100% concordance with gold-standard real-time PCR (RT-PCR). These results highlighted the potential of g-CURS to replace RT-PCR by offering rapid (within 30 min), highly specific [minor mutation discrimination of only six nucleotides (nts)], and highly sensitive (subfemtomolar) detection of target nucleic acids, removing the need for bulky equipment or thermal cycling. Furthermore, to verify the capability of g-CURS for the detection of other analytes, proinflammatory cytokines, such as interleukin (IL)-6, interferon (IFN)-gamma, and tumor necrosis factor (TNF)-α in EVs were selected as protein targets. Compared with commercial ELISA kits, g-CURS reduced the assay time from 6 h to 1.25 h, while improving sensitivity to the subpicomolar level. Specifically, it was able to control the clinical sample volume for detection to the microliter level, regardless of the number of target proteins being tested, while enabling the detection of multiple analytes. Compared with ELISA, g-CURS uses a specific sensing interface on glass fibers, enabling the capture and separation of multiple targets within the same sample and significantly reducing sample consumption and increasing sensitivity. It successfully detected cytokines in EVs from 12 PD clinical serum samples, demonstrating its superior performance in detecting low-abundance proteins. Thus, our approach simplifies the biosensing of diverse analytes by CRISPR/Cas. By integrating g-CURS-assisted nucleic acid

and protein detection into a cohesive portable platform, this methodology provides a simple and reliable solution for precise biomarker discovery from genotype to phenotype in specific clinical samples adaptable to POC testing (POCT).

Results

Ligation-based target recognition

To simplify the CRISPR/Cas-based nucleic acid-biosensing process, we implemented a ligation-based target recognition strategy. This approach eliminated the need for PAM-site screening associated with dsDNA activators and simplified crRNA design for each target DNA analyte by using a fixed ssDNA activator. The Δ157-158 mutation site in the Delta variant was selected to evaluate the feasibility of the strategy, with the corresponding wild-type (WT) serving as the control group. This 6-nt deletion in the spike-coding region, introducing NTD-specific E156G/Δ157-158, enhances the infectivity of SARS-CoV-2 and reduces its sensitivity to vaccine-induced antibodies [38]. Sequence alignment of the spike-coding regions was performed using SnapGene 6.0.2 (Figure S1A in the supplemental information online). The probe design was tailored for detecting target ssDNA (Figure 2A). Biotinylated probes (BPs; Figure 2A, purple) and amplified probes (APs; Figure 2A, orange and red sequences) were intricately engineered with multiple functional elements to identify target cDNA and with appended tags to facilitate subsequent signaling processes. All probe sequences are detailed in Table S1 in the supplemental information online. Within the BPs, a segment that complemented the ssDNA target was modified with biotin at the 5' end to enable subsequent purification. The APs were designed with a phosphate modification at the 5' end to facilitate ligation and incorporated a 23-nt tail. This tail (red segment) was strategically positioned after a region that complemented the ssDNA segment at the 3' end, drawing inspiration from previous research [30] to initiate CRISPR/Cas12a cascade amplification. Typically, two perfectly matched adjacent complementary ssDNA regions were incorporated into the probes to facilitate recognition and connection by T4 DNA ligase.

We first studied the specificity and ligation efficiency of our approach. Delta-APs and Delta-BPs were specially designed to detect the Delta spike coding sequence; thus, only the existence of the Delta target (tDelta, Figure 2B, lane 2; the 20-base pair DNA ladder is lane 1) could generate the corresponding ligated products, thereby verifying the ability of T4 DNA ligase to discriminate the highly homologous sequences from WT variants (tWT, Figure 2B, lane 3), as shown by denaturing polyacrylamide gel electrophoresis (dPAGE). Delta-APs (Figure 2B, lane 4) and Delta-BPs (Figure 2B, lane 5) were highly efficiently ligated using T4 DNA ligase with the tDelta. The ligation product is indicated by the red arrow in Figure 2B. In the absence of tDelta, no band of the correctly sized ligated products was observed (Figure 2B, lane 7).

The AP and template sequences for subsequent detection in the CRISPR/Cas-induced cascade reaction were similar in size (Figure S2 in the supplemental information online), making it difficult to distinguish the AP and template on dPAGE. Therefore, the AP sequence shown in Figure 2B was lengthened to facilitate characterization. The results indicated that neither the length nor the 5' end tail of the AP sequence significantly affected the ligation efficiency. Notably, alongside the presence of ligation products, a discernible decrease in the intensity of bands corresponding to the reactants Delta-APs and Delta-BPs was observed compared with the standard concentration. This was not observed in the WT ligation mixture.

To assess the universality of this method, we designed and validated probes for another representative infectious disease, HPV16, while using HPV18 (Figure S3A in the supplemental information online) as an interference agent within the detection system. Analysis via dPAGE demonstrated that the AP16 and BP16 probes, specifically designed for HPV16 E7, produced

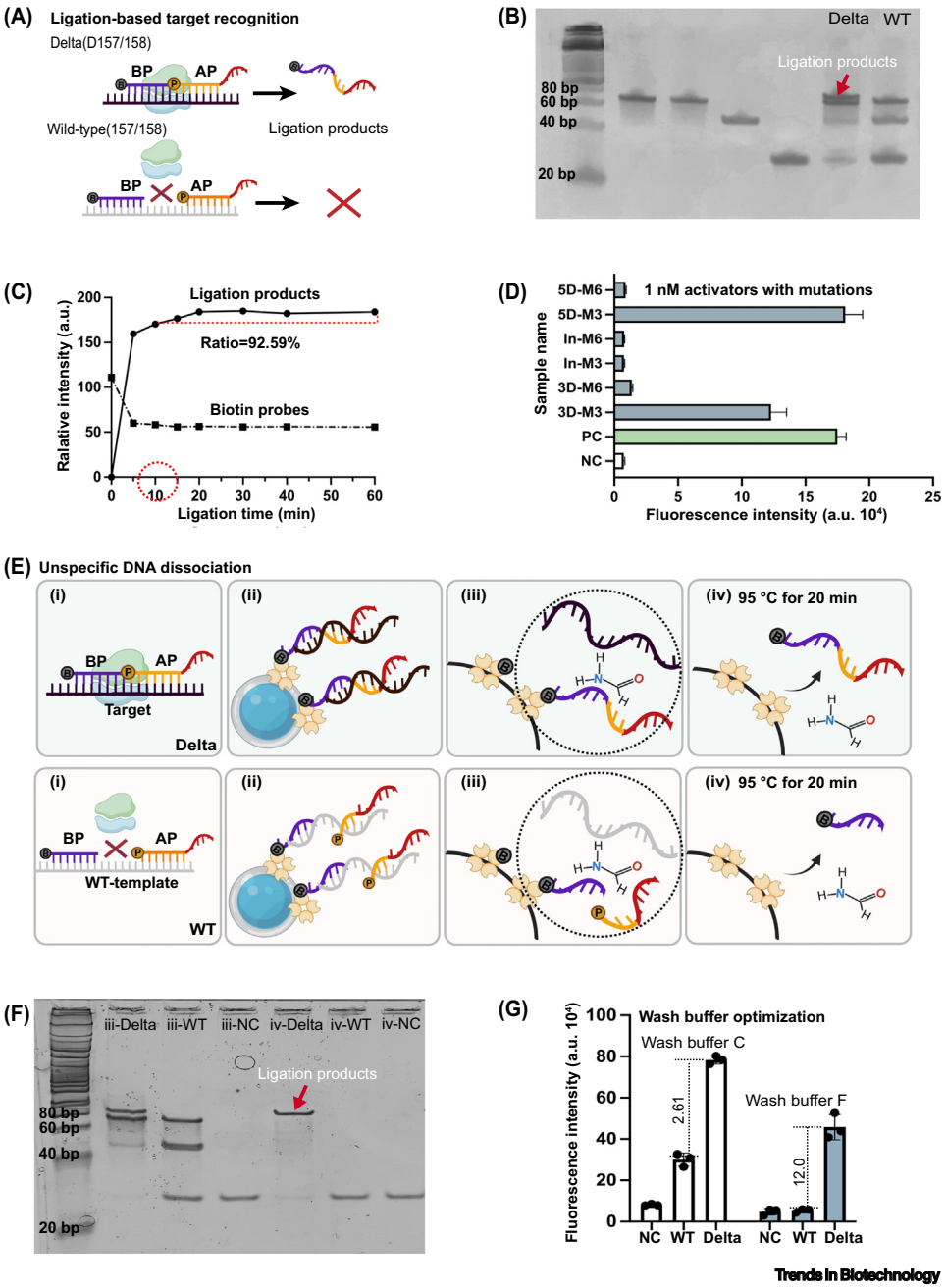


Figure 2. Ligation-based target recognition. (A) Primer design for ligation-mediated nucleic acid target recognition. D157/158 indicates the *E156G/A157–158* mutation, with a six-nucleotide (nt) deletion in the coding region. (B) Comparison of ligation results between target single-stranded (ss)DNA (Delta) and highly homogenous sequences [wild-type (WT) 6-nt difference]. Red arrow indicates the specific ligation products. (C) Optimization of ligation time with the Delta template. The relative intensity was acquired by the analysis of bands on denaturing polyacrylamide gel electrophoresis (dPAGE), acquired by ImageJ online. (D) Mutation tolerance of a ssDNA activator reduced the high specificity of CRISPR/Cas-based detection. 'Sample name' indicates the different mutation sites in the ssDNA activator: 3D-M3, 3-nt mutation in the 3′ end of the ssDNA activator; In-M3, 3-nt mutation in the interval of the ssDNA activator; NC, negative control, where ddH_2O was used as the target template; PC, positive control, which contained a ssDNA activator. (E) Schematics of T4 ligase-mediated nucleic acid target recognition (step i), formamide-assisted purification process (steps i, ii), and verification of purification results (step iv).

(Figure legend continued at the bottom of the next page.)

ligation products exclusively in the presence of the HPV16 E7 template (Figure S3B), with no nonspecific products detected in the presence of the homologous sequence HPV18 E7 (Figure S3C). Consequently, target recognition mediated by T4 ligase ensured that the fixed ssDNA activator related to the subsequent CRISPR/Cas-assisted amplification was embedded in the target DNA-based ligation product without the need for crRNA design and screening processes specific for each target. ImageJ was used to analyze the bands of the ligation product on dPAGE to optimize the ligation time. The Delta analyte-mediated ligation achieved ~92% of its plateau within 10 min (Figure 2C). The ligation reaction time for the HPV16 target plateaued within 5 min (Figure S3D). The dPAGE results indicated that extending the ligation reaction time did not lead to nonspecific ligation products (Figure 2B and Figure S3B). In addition, no ligation products were observed in the presence of highly homologous sequences used as templates (Figure 2B and Figure S3C).

The ssDNA activator alone demonstrated mutation tolerance despite variations in Cas enzymatic efficiency resulting from mutations at different positions compared with the optimal substrate [positive control (PC); Figure 2D]. These mutated sequences still significantly induced Cas-based signal amplification, as shown by the performance of samples 3D-M3 and 5D-M3 (Figure 2D). The design of the various mutation sites in the ssDNA activator and the corresponding reaction kinetic curves are detailed in Figure S4 in the supplemental information online. Thus, shifting the target recognition task to T4 ligase avoided issues such as mutation tolerance in the ssDNA activator with reduced specificity in CRISPR/Cas-based detection and limited PAM site accessibility for dsDNA activators in the CRISPR/Cas-assisted nucleic acid biosensing system. Together with the dPAGE results, this showed that the target recognition strategy effectively addressed the limitations associated with ssDNA activator-mediated CRISPR/Cas nucleic acid-biosensing systems.

However, during experimental verification, we observed that, although no ligation products were detected in the WT by dPAGE, its fluorescence signal was higher than that of the ultrapure water used as a negative control (NC) under identical conditions. We hypothesized that, although the probes were not ligated by ligase in the WT reaction system (Figure 2Ei), strong binding between the probes and the interfering template via hydrogen bonding prevented complete removal from the SA-functionalized solid interface [magnetic beads (MBs) or glass fibers], leading to minor residual APs and a signal higher than the NC. Therefore, we investigated the recipe of wash buffers (Table S2 in the supplemental information online) effective for AP removal, a critical optimization aimed at enhancing the signal-to-noise ratio. Previous work showed that formamide effectively reduced the Tm value by disrupting hydrogen bonds in a linear manner [39]. Thus, after T4 ligase-mediated ligation, the Delta template-mediated ligation product and the WT template-AP-BP ternary complex were captured by SA-MBs (Figure 2Eii). Theoretically, only BP would remain on the SA-MBs in the NC sample. At the same time, in the Delta sample, a duplex of the ligation product and template would be present, while a ternary complex would form via hydrogen bonding between AP, BP, and the WT template. The product coated-MBs were purified by wash buffer F (30% formamide in wash buffer C) at 37°C for 5 min, which theoretically dissociated the AP from the WT complex (Figure 2Eiii).

(F) Characterization of the purification process (steps iii, iv) of Delta cDNA, WT, and NC on dPAGE. To assess the specific ligation product and purification efficiency in the presence of formamide, biotinylated sequences (lanes 5–7) were dissociated from the streptavidin–magnetic beads (SA-MBs; step iv). (G) Comparison of purification efficiency between a formamide-containing buffer (wash buffer F) and a formamide-free buffer (wash buffer C). The endpoint fluorescence intensity was measured within 30 min using linear reporter (LR)-assisted CRISPR/Cas-mediated cyclic amplification following the purification step with different wash buffers. Data are mean ± standard deviation (SD) (N = 3). (E) Created with BioRender (biorender.com); for image licenses, please refer to the supplemental information online. Abbreviations: AP, amplified probe; BP, biotinylated probe.

The Delta sample clearly showed distinct ligation products, while no corresponding bands appeared in the WT or NC lanes, confirming the specificity of ligation (Figure 2F, lanes 2–4). Although some ligation products were lost due to formamide disrupting SA-biotin binding (which relied primarily on hydrogen bonding [40]), this loss could be minimized by optimizing wash time, functional temperature, and formamide concentration. The visible presence of AP in the wash solution from WT MBs (Figure 2F, lane 2) supported the hypothesis that incomplete AP removal led to the formation of a ternary complex with BP and the WT template, raising the background signal compared with the NC. To confirm the effectiveness of these wash steps and the specificity of the ligation-based strategy, the MBs were heated at 95°C for 20 min in a 50% formamide-containing solution, and the supernatant solutions were collected for electrophoresis verification (Figure 2Eiv). Lane 5 (Figure 2F) contained the boiled supernatant from the *Delta* sample, thus showing only ligation products. Meanwhile, lane 6 (WT sample; Figure 2F) was consistent with the NC result, showing that only BP remained on the MBs. These electrophoresis results verified that the nonspecific AP was completely removed by wash buffer F, and that adding formamide to the wash buffer eliminated nonspecific interference from hydrogen bond-mediated coupling. Thus, by optimizing the concentration of formamide in the wash buffer, we could effectively remove the pairing of APs with highly homologous sequences of the non-test target, achieving high specificity.

To make the system suitable for a POCT scenario, we replaced SA-MBs with SA-functionalized glass fibers (SA-glass fibers) in subsequent experiments after validating the purification method with MBs. Although nucleic acid conjugation on the fiber platform exhibited a slight decrease in efficiency compared with homogeneous MBs, it remained effective for detecting E7 cDNA (Figure S5 in the supplemental information online) and, considering the picomolar limit of detection of our linear reporter system, confirms the potential of SA-modified fibers to capture target nucleic acids; future enhancements and clinical testing will focus on removing reliance on MB separation and enabling multiplexed detection using the fiber-based platform. Under optimized conditions, a 10% formamide-containing wash buffer F was ultimately selected for SA-glass fiber purification (Figure S6 in the supplemental information online). Thus, the signal-to-noise ratio between highly homogenous sequence-WT and target *Delta* increased from 2.61 to 12.0 (Figure 2G).

g-CURS-assisted nucleic acid detection

Having addressed the limitations of ssDNA activator-mediated CRISPR/Cas nucleic acid-biosensing systems, including their specificity and the complex crRNA screening required for each target DNA, the next step was to determine the sensitivity of g-CUSR to detect low-abundance analytes. A preamplification-free strategy based on CR-mediated cascade amplification techniques previously used in the AutoCAR system [30] was adopted. The CR includes a 21-nt ssDNA outer circle and an 18-nt complementary inner circle sequence. The outer circle, with its small size, forms a rigid structure, preventing Cas12a and crRNA complexes [Cas12a ribonucleoprotein (RNP)] from generating an R-loop and subsequentially causing nontarget activation before target binding. The inner circle sequence, modified with a quencher at the 3' end and a fluorescent group at the 5' end, pairs with the outer circle. After hybridization, the proximity (3 nt) enables fluorescence quenching via fluorescence resonance energy transfer (FRET). The 3-nt TTT segment in the outer circle serves as the preferred substrate for the activated Cas12a RNP, which cleaves the TTT site upon target DNA presence, linearizing the CR. The linearized dsDNA, matching the target and containing a PAM site, serves as a substrate for further Cas12a activation, initiating signal exponential accumulation [30].

Before applying CR (21 nt in size) in g-CURS, the synthesis of a small circle was optimized. To improve the efficiency of small ssDNA circle cyclization (~20 nt), a method using base-stacking

interactions between the dumbbell hairpin structure (Hc) and the linear outer circle sequence (Lc, 21 nt) was used (Figure 3Ai) [41]. Hc, featuring hairpin structures (dark blue) at both ends and a central splint sequence (light green) complementary to Lc, hybridizes with the ends of Lc (dark green) to form a stable DNA duplex, enhancing T4 ligase efficiency. To validate the efficiency of the cyclization, two commonly used methods described by Deng and coworkers were tested as controls [30]. First, we tested the method of directly using a short splint strand (Sc) identical to the central segment of Hc to form the small circle (Figure 3Aii). However, Sc-Lc interactions often resulted in repeated (Sc-Lc)*n* states due to electrostatic repulsion [41], producing dimeric or polymeric circles instead of monomers. Second, we evaluated click chemistry-based ligation methods for constructing circular structures from short DNA sequences (~20 nt) (Figure S7A in the supplemental information online). However, based on dPAGE analysis, the method was not suitable for the formation of small circles and exhibited low yields with no discernible target products visible on the dPAGE gel (Figure S7B,C).

Thus, the Hc-assisted circle formation method [41] was selected to construct the desired 21-nt ssDNA circles. Comparison of Hc-assisted small circle formation products and Sc-assisted small circle formation products on dPAGE (Figure 3B, lane 5) demonstrated that Sc-mediated cyclization products resulted from the reaction catalyzed by T4 DNA ligase. However, instead of a distinct 21-nt circle band, a significant amount of by-products, such as dimeric or polymeric circled products, was observed (Figure 3B, lane 5), indicating that the desired cyclized product (monomeric ones) yield was extremely low and was not the dominant product resulting from the use of T4 ligase and Sc. This outcome aligned with theoretical predictions, given that the Lc sequence length was only 21 nt, which inherently limited T4 ligase-assisted cyclization efficiency [42]. Conversely, base-stacking interactions between Hc and Lc facilitated duplex formation (Lc-Hc), enhancing ligation efficiency with T4 DNA ligase and successfully producing monomeric small ssDNA circles (Figure 3B, red arrows in lanes 7 and 8). These small circles (~20 nt) exhibited higher mobility compared with their linear counterparts due to their rigid structure, as reported previously [43]. Exonuclease I and III digestion confirmed cyclization by selectively degrading unreacted linear sequences, leaving circular products that were resistant to digestion. Lc-Sc ligation produced primarily large circles (Figure 3B, lane 6), while Lc-Hc ligation predominantly formed monomeric circular DNA (Figure 3B, lane 8).

To further verify the feasibility of the base-stacking strategy, we analyzed interactions between Hc-Lc and Sc-Lc duplexes in a ligase-free system using NuPAGE. The gel displayed migration patterns for Sc, Hc, Lc, Sc-Lc, and Hc-Lc duplexes (Figure 3C). Notably, intermediate products (red arrow) were observed only in lane 6 (Hc-Lc), indicating Hc-Lc duplex formation driven by base stacking, while no intermediates were detected in lane 5 (Sc-Lc). In addition, to confirm the universality of this method, an alternative set of Sc2, Lc2, and Hc2 was tested using the same procedures, with similar results, with only Hc2-Lc2 driving efficient monomeric circle formation (red arrows in lanes 7 and 8 of Figure S8A and lane 6 of Figure S8B in the supplemental information online).

Following Hc-assisted circle formation, ssDNA monomeric circles were purified using exonucleases and a 10K molecular weight Amicon-Ultra column and collected from the lower layer of the column (Figure S9A in the supplemental information online). A standard curve was established to quantify the circles by serially diluting Lc, staining with the nucleic acid-specific dye SYBR Green I, and measuring the fluorescence signal (Figure S9B). The concentration of purified circles was determined using the standard curve from SYBR Green I staining (Figure S9C) rather than the UV absorption value (Figure S8D). The latter estimation was higher than the initial Lc concentration due to the impact of the small amino acid molecules released from inactivated enzymes.

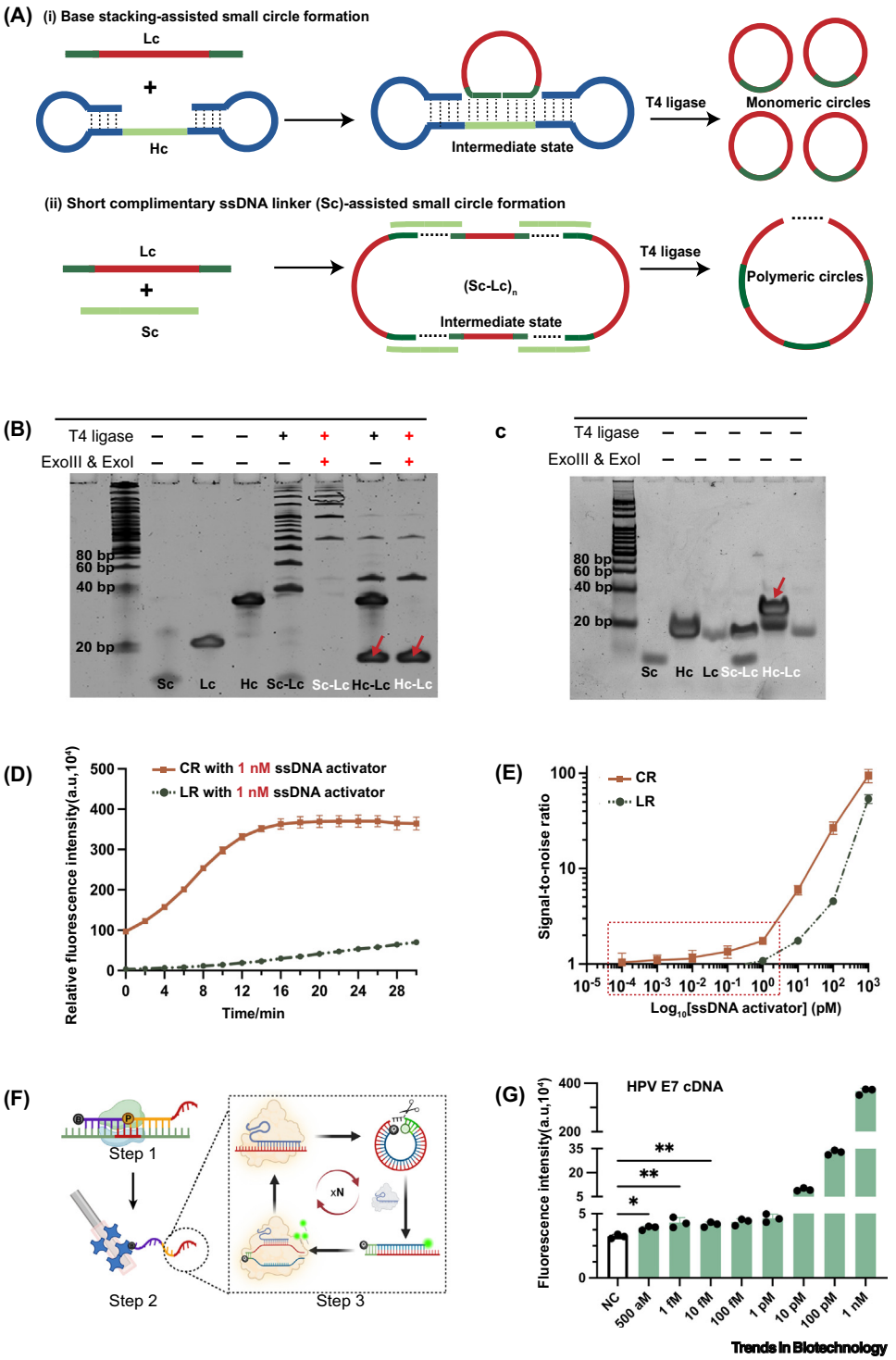


Figure 3. Glass-fiber interfaced CRISPR/Cas with a universal reagent setting (g-CURS)-assisted nucleic acid detection. (A) Schematics of base stacking-assisted (Hc)-small circle formation and short complementary single-stranded (ss)DNA linker (Sc) assisted-small circle formation. (B) Characterization of Hc-assisted small circle formation products and

(Figure legend continued at the bottom of the next page.)

This process facilitated the evaluation of the yield of ssDNA circle 1, calculated as ~30%. Yield varied with Lc sequences due to differing by-product proportions; for example, Lc2 generated fewer by-products and, thus, yielded higher yields (Figure S8A).

To verify batch-to-batch stability, a comparative statistical analysis of CR1 quantities was conducted across three batches. There was no statistically significant differences among the batches (*P = 0.0857, Kruskal–Wallis test;* Figure S10 in the supplemental information online). In addition, the hybridization time between the inner and outer circles was observed to have no significant impact on the signal-to-noise ratio. Therefore, the purified monomeric circle was hybridized with the inner circular sequence at equal concentrations at 95°C for 5 min to complete the hybridization (Figure S11A in the supplemental information online) and then gradually cooled to room temperature. The achieved CRs were stored at 4°C for subsequent experiments.

To assess the performance of g-CURS using CRs for low-abundant analyte detection, we initially used a 1 nM ssDNA activator to evaluate the kinetics of the system in homogeneous solutions. The cascade amplification mediated by the CR exhibited first-order rate kinetics, and its relative fluorescence signal increased exponentially, plateauing within 15 min, indicating significant enhancement of the enzymatic reaction speed (Figure 3D, red curve). By contrast, the LR displayed linear signal growth over time (Figure 3D, green curve). To minimize errors resulting from detection delays caused by initiation, we also used an endpoint method to eliminate discrepancies (Figure S12 in the supplemental information online). After optimizing reaction conditions (Figure S11B,C), CR-mediated amplification outperformed LR-mediated amplification within 30 min, with the detection range extended by five orders of magnitude and the detection limit improving from 1 pM to 10 aM in homogeneous solutions (Figure 3E). Comparison of CRISPR/Cas12a nucleic acid biosensing between CR and LR with a 15-min reacting duration (Figure S13 in the supplemental information online) and the resulting kinetic curves (Figure 3D) showed that g-CURS demonstrated ultra-high sensitivity.

To demonstrate the suitability of g-CURS for POCT, the functionalized sensing interface was fabricated on glass fibers, integrated with 4-aminobenzoic acid-modified gallium-indium eutectic nanoparticles (EGaIn-PABA) as reported in a previous study [35]. EGaIn-PABA was characterized by a zeta sizer showing ~300 nm and a zeta potential of ~40 mV, which was consistent with previous work [44] (Figure S14A,B in the supplemental information online). EGaIn-PABA was successfully modified on a glass fiber surface under scanning electron microscopy (Figure S14C). The presence of the elements Ga, In, C, and O was confirmed by energy-dispersive X-ray spectroscopy characterization (Figure S14D). The EGaIn-PABA-functionalized fiber surface provided terminal carboxylic acid groups for protein (SA or capture antibody) immobilization [45]. Analysis of SA-glass fibers incubated with a 200 nM biotinylated fluorescence probe (BF probe) showed uniform signals only in the BF probe-incubated SA-glass fibers, with no fluorescence in controls, confirming successful SA coupling (Figure S15 in the supplemental information online). After T4 ligase-assisted target recognition, SA-glass fibers were then used to capture the biotin-labeled

short Sc-assisted small circle formation products on denaturing polyacrylamide gel electrophoresis (dPAGE). (C) Characterization of intermediate states of Hc-assisted small circle formation and short Sc-assisted small circle formation on native PAGE (NuPAGE). (D) Comparison of the kinetic curve between the circular reporter (CR) and linear reporter (LR) with a 1-nM ssDNA activator trigger. (E) Comparison of CRISPR/Cas12a nucleic acid biosensing between CR and LR. (F) g-CURs-assisted CRISPR/Cas12a nucleic acid detection mechanism. (G) Sensitivity of synthetic human papillomavirus (HPV)16 E7 cDNA detection using g-CURS within 15 min. Data are mean ± standard deviation (SD) (N = 3); statistical significance was determined using one-way ANOVA: *P <0.05; **P <0.01. (F) Created with BioRender (biorender.com); for image licenses, please refer to the supplemental information online.

ligation product and served as the sensing interface for subsequent CR-assisted CRISPR/Cas signal amplification (Figure 3F). To balance the signal-to-noise ratio and rapid detection requirement, a 15-min reaction time was selected for CR-mediated CRISPR/Cas amplification (Figure S16 in the supplemental information online). Under optimized conditions, g-CURS detected synthesized HPV16 E7 cDNA with a detection limit of 500 aM within the 15-min amplification period (Figure 3G), matching the sensitivity of gold-standard RT-PCR for low-abundance nucleic acids (Figure S17 in the supplemental information online). Similarly, it achieved a 750 aM detection limit (~450 copies/μl, Figure S18 in the supplemental information online) for the Delta spike protein-coding segment under the same rapid workflow. This performance aligns with clinical requirements, given that SARS-CoV-2 viral loads in children are marginally lower than in adults (≤0.5 $\log_{10}$units), reaching ~78% of adult peak infectivity. Notably, 8% of cases exhibit ≥10^9 copies/swab, while adults attain peak viral loads of ~10^8 copies/swab at 4.3 days post infection [46].

g-CURS-assisted protein detection

Integration of g-CURS with an immunoassay using the fixed pair of ssDNA activators and crRNA for detection of nucleic acids can also enable multiprotein detection by modifying the dAb with ssDNA to trigger the CRISPR/Cas system [35]. Thus, using an optimized 1:100 dilution ratio of dAb-ssDNA (Figure S19 in the supplemental information online), g-CURS was used to detect three proinflammatory cytokines (IL-6, TNF-α, and IFN-γ) in low abundance within a 15-min signal amplification duration. The g-CURS system achieved the lowest detection limit (LoD) for IL-6 of 0.1 pg/ml and a linear detection range of 1–100 pg ml^{-1}, in contrast to that of commercial IL-6 ELISA kits (3.13 pg/ml, 3.13–300 pg/ml) (Figure 4A; Figures S20A, S21A, and S22 in the supplemental information online) The LoD for IFN-γ was 0.1 pg/ml (linear range: 1–100 pg/ml), compared with the 15.6–1000 pg/ml range of IFN-γ ELISA kits (Figure 4C; Figures S20C, S21C, and S23 in the supplemental information online). Similarly, the detection limits of 0.1 pg/ml for TNF-α (linear range: 0.5–100 pg/ml) outperformed commercial TNF-α ELISA kits (linear range: 15.6–1,000 pg/ml) (Figure 4E; Figures S20B, S21B, and S24 in the supplemental information online). Thus, g-CURS-assisted protein detection significantly enhanced the sensitivity to the subpicomolar level, surpassing the performance of commercial ELISA kits (Figure 4B,D,F). These findings highlight the potential of the g-CURS system for detecting low-abundance proteins. For specificity testing, we spiked various nonspecific proteins at 10 pg/ml as substitutes for IL-6, TNF-α, and IFN-γ. Cross-reactivity with nonspecific proteins was <10%, with a distinct response observed for the target analytes, demonstrating minimal interference in detection of the target biomarkers (Figure S25 in the supplemental information online).

Clinical sample detection by g-CURS

As detailed earlier, g-CURS demonstrated the ability to detect diverse analytes (nucleic acids and proteins) using a standardized reagent setting of glass fiber interfaced-CRISPR/Cas biosensing. Following sample pretreatment to extract DNA and proteins from clinical samples, the glass fiber sensing interface allowed independent reactions and signal outputs for each target (Figure 5A). Specificity for nucleic acid detection was achieved through ligation-assisted target recognition, with the ligation products captured by SA-glass fibers, enabling concurrent detection of multiple nucleic acids. Specificity for protein detection was realized by immunoassays, with each fiber dedicated to a specific protein. Using the CR-mediated CRISPR/Cas amplification system, a portable g-CURS device [35] (Figure S26 in the supplemental information online) was used to report the signal, enabling the simultaneous detection and analysis of multiple targets with super high sensitivity for POCT (Figure 5A). The microchannel chip (Figure S26A,B) enabled separate detection of multiple analytes (Figure S26C), with the amplification reagent mixture prestored in each channel, simplifying the detection process and reducing reagent use. Images from the channels of the detection chip were analyzed using a gray-scale value to correlate with fluorescence

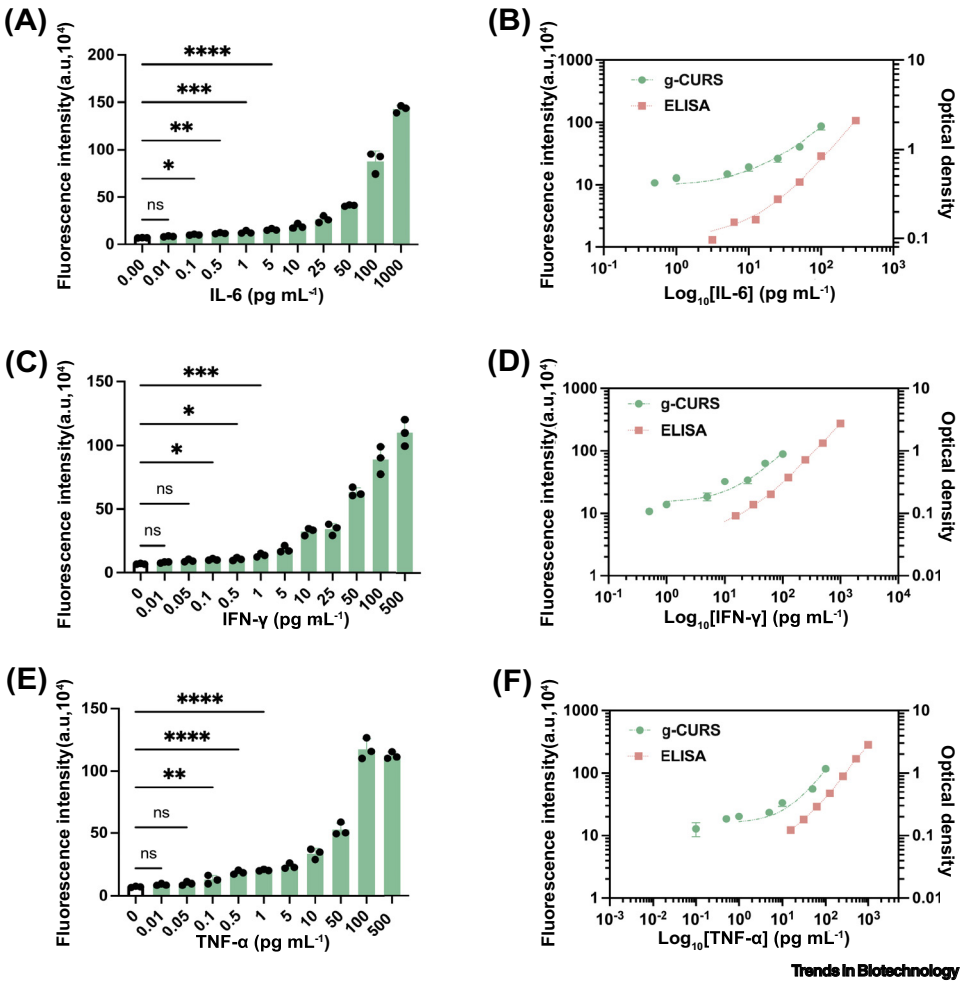
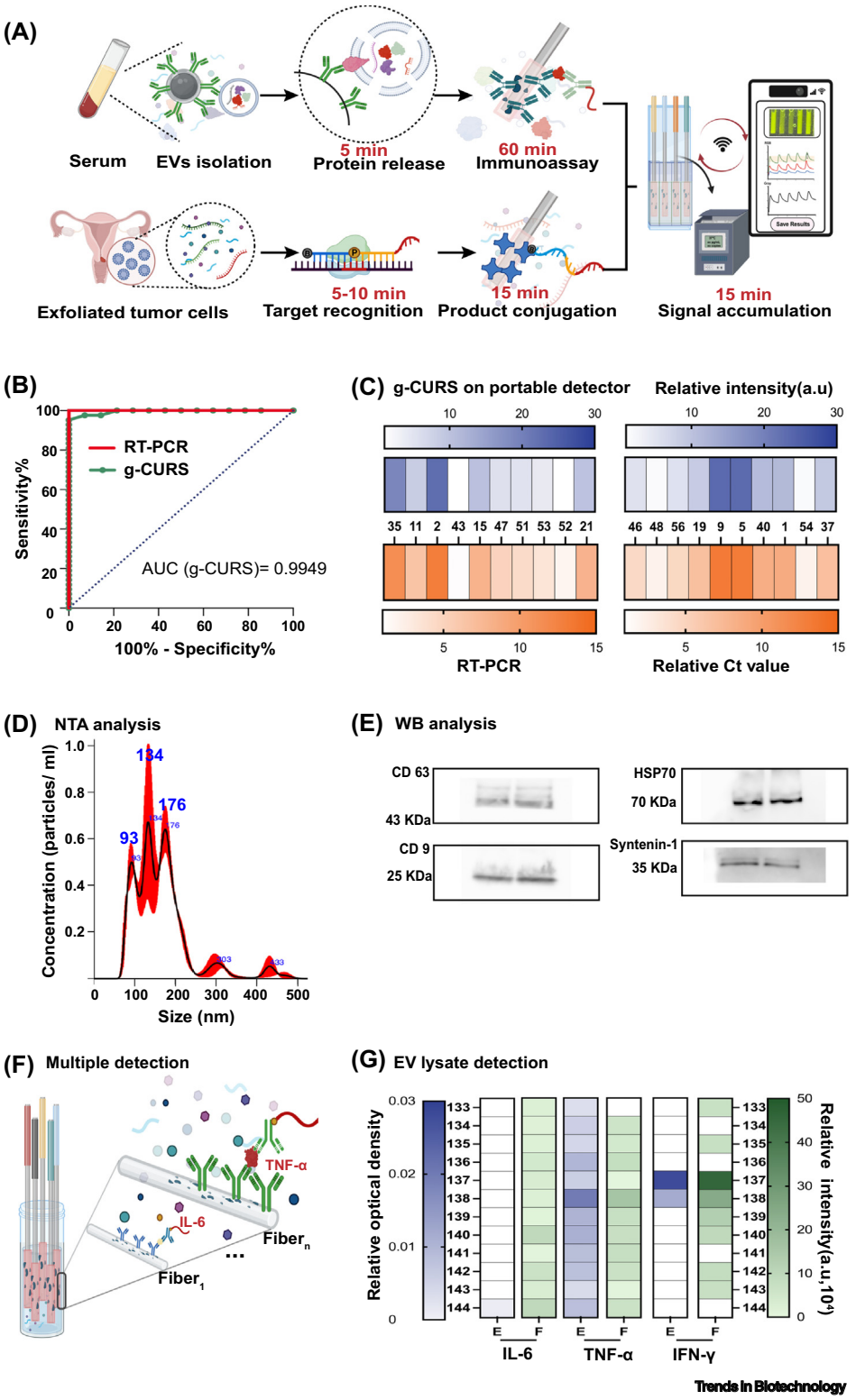


Figure 4. Glass-fiber interfaced CRISPR/Cas with a universal reagent setting (g-CURS)-assisted protein detection. (A,C,E) Range of detection of g-CURS for interleukin (IL)-6, tumor necrosis factor (TNF)-α, and interferon (IFN)-γ. (B,D,F) Comparison of the linear detection range of commercial ELISA kits versus g-CURS for detecting IL-6, TNF-α, and IFN-γ. Data are mean ± standard deviation (SD) (N = 3); statistical significance was determined using one-way ANOVA: *P <0.05; **P <0.01; ***P <0.001; ****P <0.0001, ns, not significant.

intensity, and these values from each channel were used to determine target analyte concentrations based on the calibration curve relating fluorescence intensity to the logarithm of the target analyte concentrations (Figure S26D). Our fluorescence analysis relied on calibrated camera-captured images to ensure a consistent depth of field and size, allowing for establishment of an accurate calibration curve. By analyzing the entire fixed area of the images and utilizing a source code that sets an appropriate grayscale threshold, we effectively mitigated the effects of particles and eliminated scratches and noncircular noise points. Meanwhile, statistical methods ensured that excessively bright spots caused by noise were accounted for and that the original readings remained within a reliable range. Representative chip analysis (Figure S27 and Note S1 in the supplemental information online) with further verification achieved using ImageJ software (Figure S28 and Note S2 in the supplemental information online) revealed that the proportion of noise above the threshold was <5%; thus, the mean value served as a reliable final reading.



(See figure legend at the bottom of the next page.)

To demonstrate the clinical applicability of g-CURS for the detection of various biomarkers, clinical samples from patients with hrHPV were used for validated nucleic acid detection. A cohort of 56 HPV16-cervical swab samples provided by Sun Yat-sen University Cancer Center with ethics approval were tested after reverse transcription, with RT-PCR identifying 42 as HPV16 E7 sequence positive and 14 as negative (Table S3 in the supplemental information online). By comparison, g-CURS assays detected 42 out of 42 (100%) HPV16-positive samples and 14 out of 14 (100%) HPV16-negative samples. Significant correlations among the RT-PCR and g-CURS assays were found (Figure S29 in the supplemental information online). Notably, the g-CURS-assisted HPV16 E7 detection between healthy controls and positive groups achieved an impressive area under the receiver operating characteristic curve (AUC) of 0.9949, reflecting a reliable clinical sample detection ability (Figure 5B). To validate rapid detection on an integrated portable device, 20 representative samples from the cohort (Figure S18E) were then tested, achieving 100% detection accuracy with g-CURS on the portable device (Figure 5C). Typically, by capturing ligation products from each specific target DNA on separate glass substrates and creating an independent reaction surface for each target, g-CURS has the ability to generate distinct detection signals and enable the simultaneous detection of multiple nucleic acids.

For multiple protein detection by g-CURS, EVs were isolated from a cohort of 12 serum samples provided by Qilu Hospital of Shandong University with ethics approval. Three proinflammatory cytokines (IL-6, TNF-α, and IFN-γ) included in PD EVs were chosen as the analytes to verify the potential of g-CURS to detect low-abundance proteins. Previous research showed a correlation in transmembrane protein expression between cerebrospinal fluid and brain-derived EVs [47], with CD81 being more highly expressed compared with CD63 and CD9. Therefore, CD81-functionalized MBs were prepared to capture CD81-positive EVs in the serum of patients with PD. Western blot (WB) and nanoparticle tracking analysis (NTA) were used to validate the success of EV capture in accordance with EV study guidelines. EVs isolated using anti-CD81 MBs were analyzed via WB. Tetraspanins CD9, CD63, heat shock protein 70 (Hsp70), and syntenin-1, which are well-established positive EV markers, were used to characterize isolated EVs (Figure 5E and Figure S30 in the supplemental information online). CD9, CD63, Hsp70, and syntenin-1 expression in the two PD samples indicated the successful capture of EVs by anti-CD81 MBs, facilitating subsequent detection and analysis. While WB offered valuable evidence for EV validation, complementary techniques were necessary for comprehensive EV characterization. NTA revealed that the mean size of CD81-positive EVs was 164.3 ± 4.7 nm, consistent with the typical EV size range of 30–1000 nm [47,48]. The particles had a relatively high concentration of $8.71 \times 10^9 \pm 6.91 \times 10^8$ particles/ml (Figure 5D). To achieve statistical significance, NTA data from additional patients with PD were randomly selected (Figure S31 in the supplemental information online). The NTA results indicated that the mean size of CD81-positive EVs was ~170 nm with a relatively high particle concentration, consistent with the results in Figure 5D.

Figure 5. Clinical sample detection by glass-fiber interfaced CRISPR/Cas with a universal reagent setting (g-CURS). (A) Flowchart of various types of analyte detection (nucleic acid and proteins). (B) Receiver operating characteristic curve (ROC) of g-CURS-assisted human papillomavirus (HPV)16 clinical sample detection, with real-time PCR (RT-PCR) as the standard reference. (C) Testing of representative E7 clinical samples and comparison of the results from RT-PCR and g-CURS using a portable device. The relative control (Ct) value was calculated by subtracting the blank value from the Ct value and then taking the absolute value of the result. (D) Nanoparticle tracking analysis (NTA) results of extracellular vesicles (EVs) isolated from serum samples from patients with Parkinson's disease (PD). (E) Western blot (WB) results from the representative proteins isolated from EVs. (F) Glass fibers functionalized with specific capture antibodies enabled the simultaneous detection of multiple proteins within the same clinical sample, facilitating accurate analysis using a minimal sample volume. (G) Comparison of representative cytokine detection in EVs from patients with PD using commercial ELISA kits versus the g-CURS system. E indicates the ELISA results, and F represents the g-CURS system results. (A,F) Created with BioRender (biorender.com); for image licenses, please refer to the supplemental information online. Abbreviations: AUC, area under the receiver operating characteristic curve; IFN, interferon; IL, interleukin; TNF, tumor necrosis factor.

The EVs captured by CD81-functionalized MBs were lysed using the protocol described by Li and coworkers [47] to release their contents for detection. The samples were then diluted tenfold to detect IL-6, TNF-α, and IFN-γ. The EV lysates were analyzed by commercial ELISA kits and the g-CURS system. To realize the simultaneous detection of multiple targets in a single sample, glass fibers modified with IL-6-, TNF-α-, and IFN-γ-capture antibodies were immersed into the single clinical sample diluted solution concurrently (Figure 5F). In addition, the remaining EV lysate solution was diluted at the same ratio and evenly divided into three portions for individual protein detection using the corresponding ELISA kits. Clinical test results demonstrated that the g-CURS assay provided superior sensitivity for protein detection in EVs (Figure 5G) compared with commercial ELISA kits. From the clinical detection signal response (Figure 5G), no IL-6 was detected in the EVs of 12 samples using ELISA, while g-CURS results revealed a detectable signal. By substituting this signal into the corresponding linear equation for IL-6, the concentration of IL-6 in diluted EVs was successfully calculated for six patient samples (Figure S32 and Table S4 in the supplemental information online). The concentrations of the remaining six samples could not be determined because they exceeded the linear range (1–100 pg/ml). For TNF-α, both methods showed a positive signal response (Figure 5G). However, the LoD values of all 12 samples, which fell outside its linear range (15.6–1000 pg/ml), were too low to be determined by ELISA. By contrast, g-CURS results provided TNF-α concentrations for eight samples, indicating that their levels were <15.6 pg/ml (Table S4), which is consistent with the previous ELISA findings. For IFN-γ, significant results were only observed in patients 137 and 138 using ELISA (Figure 5G). By contrast, g-CURS successfully calculated the IFN-γ concentrations for eight EV samples (Table S4). The g-CURS system uses independent functionalized fibers to capture individual target proteins within each sample (Figure 5F), enabling the detection of multiple targets with a small sample volume requirement (5 μl EV lysate for multiple protein detection).

Thus, the g-CURS system advances CRISPR/Cas biosensing by enabling ultrasensitive and highly specific detection of diverse nucleic acids and proteins in clinical settings while reducing reaction time and sample volume requirements. When integrated with a portable device, g-CURS shows great potential for POCT, enhancing the efficiency and accuracy of clinical diagnostics.

Discussion

In precision medicine, there is an urgent need for versatile biosensors for comprehensive biomarker analysis to enhance diagnostic accuracy and therapeutic outcomes. However, there is still room to enhance the sensitive, specific, simplified, and cost-effective detection of various types of biomarker using current multianalyte biosensors, including liquid biopsy methods in cancer diagnostics [49] or the combined detection of inflammation markers and pathogenic nucleic acids in infectious disease diagnostics [50]. CRISPR/Cas biosensors have demonstrated significant potential for diverse biomarker detection, but require specific reagent settings for each analyte. Compared with reported CRISPR/Cas biosensing technologies for nucleic acid or protein detection (Table S5 in the supplemental information online), the g-CURS technology reported here can simplify and standardize CRISPR/Cas biosensing by addressing the knowledge gap through improving target recognition, signal cascade accumulation, and the integration of sample-to-answer portable devices in a signal platform realizing multianalytes detection. For example, g-CURS exhibits specificity down to a single nucleotide in nucleic acid detection through ligase-based target recognition strategies, the same as high-performance point mutation detection in ligase-amplification reactions and ligase-based sequencing strategies [51]. In addition, g-CURS achieves high sensitivity down to the attomole level for nucleic acid detection and the subpicomolar level for protein detection by using CR-assisted signal cascade amplification. Furthermore, g-CURS generates multiple nucleic acid detection results within 30 min and multiplexed protein analytical results within 80 min with a small volume of samples by integration

with glass fibers and a portable fluorescence reader. Finally, g-CURS realizes multianalyte detection using a standard set of crRNA and matching DNA activators for CRISPR/Cas biosensing. Thus, a one-stone–multiple-birds strategy renders g-CURS suitable for biomarker discovery of chronic diseases, such as PD, in a POC fashion.

The g-CURS system demonstrated clinical parity with RT-PCR and commercial fluorescent readers for portable HPV16 detection, validating its diagnostic reliability. However, in SNP detection applications, the inherent tolerance of T4 DNA ligase for G:T mismatches introduces false-positive risks through nonspecific ligation. This challenge is strategically resolved through oxanine-modified probes enforcing strict G:C pairing specificity [32], complemented by betaine additives to destabilize secondary structures, SSB-mediated DNA stabilization [52], and computational modeling for optimal probe design. However, a critical limitation persists in the current iteration of the system: its exclusive compatibility with single-stranded templates, given that T4 ligase lacks helicase activity for dsDNA unwinding and exhibits limited double-strand target recognition fidelity under isothermal conditions (see Outstanding questions).

Furthermore, the subpicomolar detection sensitivity of g-CURS-assisted protein biosensing could enable it to meet the demand for detection of low-abundance proteins in EVs [53]. Clinical test results showed that the g-CURS-assisted protein assay provided superior detection sensitivity for proteins in diluted EV solutions compared with commercial ELISA kits. Reducing the dilution factor or concentrating the clinical sample during pretreatment can increase analyte concentrations and improve ELISA testing. However, this also increases the demand for clinical sample collection. This becomes especially challenging when testing multiple proteins in a single patient, given that ELISA cannot separate proteins and requires a separate sample for each target. Expanding the sample volume indefinitely is impractical for clinical applications. By contrast, the g-CURS system uses independent functionalized fibers to capture individual target analytes within each sample, enabling the detection of multiple targets from a single sample. This approach significantly reduces sample collection volume requirements, with its advantages becoming even more apparent when testing multiple targets.

In future research, we aim to integrate advanced sample treatment with g-CURS to obtain both proteins and nucleic acids, utilizing the unique advantage of EVs as multicargo carriers [54–56] to achieve true sample-in–answer-out detection. With such advances, the g-CURS system has the potential to become a powerful liquid biopsy tool for the simultaneous analysis of proteins and mRNA, creating stronger connections between disease genotypes and phenotypes to enhance the accuracy of early disease diagnosis and treatment, especially in chronic diseases, such as PD.

Concluding remarks

Due to the complex interactions among biomolecules, such as proteins and nucleic acids, in disease progression, there is an urgent need for versatile biosensors capable of comprehensive biomarker analysis to improve diagnostic accuracy and therapeutic outcomes. However, current multianalyte biosensors, including liquid biopsy methods for cancer diagnostics [49] and the combined detection of inflammation markers and pathogenic nucleic acids in infectious disease diagnostics [50], require further advances to enhance their sensitivity, specificity, simplicity, and cost-effectiveness.

The versatile g-CURS platform simplifies and standardizes CRISPR/Cas biosensing for diverse analyte detection, offering a simple and reliable solution for precise disease characterization from both the genotype to phenotype in specific clinical samples. Integrating a portable detector makes it highly adaptable for POCT. Its ultra sensitivity and high specificity enable detection of

Outstanding questions

With the substitution of different ligases or the incorporation of enzymes capable of unwinding dsDNA, could g-CURS be adapted to detect a broader range of nucleic acids beyond ssDNA?

Can the g-CURS system be adapted with an efficient sample treatment module to achieve sample-to-answer detection, providing simultaneous high-throughput information from genotype to phenotype for a clinical setting?

Can the g-CURS system be integrated with mathematical algorithms to enable artificial intelligence (AI)-driven diagnoses?

various low-abundant analytes in different clinical settings, including infectious diseases or chronic diseases. With further optimization of the optical path design in the portable device and integration of sample pretreatment processes, g-CURS has the potential for broader applications across diverse POCT scenarios. We also envision further advances in the clinical application of g-CURS to enhance its preclinical and clinical utility in treatment monitoring and prognostication. This involves increasing its high-throughput capacity, enabling precise identification and classification, and simultaneously processing samples to obtain both nucleic acids and proteins within a single reaction (see Outstanding questions).

STAR★METHODS

Detailed methods are provided in the online version of this paper and include the following:

- KEY RESOURCES TABLE
- EXPERIMENTAL MODEL AND STUDY PARTICIPANT DETAILS
  - Probe information
- METHOD DETAILS
  - Ligation
  - Verification of mutation tolerance of ssDNA activator
  - Preparation of outer ssDNA circle of CRs
  - Yield estimation of ssDNA monomeric circles
  - Characterization of ssDNA monomeric circles
  - Verification of amplification capability of CRs in homogeneous solution
  - Modification and characterization of glass fibers
  - Optimization of formamide concentration in wash buffer F
- Preparation of dAb-ssDNA conjugation
  - Preparation of g-CURS for nucleic acid detection
  - Preparation of g-CURS for protein detection
  - Preparation of the detection chip in the portable device
  - Validation of HPV16 E7 mRNA in cervical tumor clinical samples by RT-PCR
  - Validation of HPV16 E7 mRNA in cervical tumor clinical sample by the g-CURS system
  - Preparation and characterization of EVs from PD serum samples
  - Validation of g-CURS-assisted protein detection in EV lysates
- QUANTIFICATION AND STATISTICAL ANALYSIS

RESOURCE AVAILABILITY

Lead contact

Requests for further information and resources should be directed to, and will be fulfilled by, the lead contact, Guozhen Liu (liuguozhen@cuhk.edu.cn).

Materials availability

This study did not generate new unique reagents.

Data and code availability

Original WB images are included in the supplemental information online. Microscopy data reported in this paper will be shared by the lead contact upon request.

All scripts are available in the supplemental information online.

Any additional information required to reanalyze the data reported in this paper is available from the lead contact upon request.

Author contributions

Methodology: G.L., T.Y., S.Z.; validation: T.Y., Y.L., Y.O., S.L., T.K.; visualization: T.Y., S.Z.; writing – original draft, and formal analysis: T.Y., G.L.; clinical sample detection support: L.S., C.S.; supervision, funding acquisition, and project administration: G.L.

Acknowledgments

The work was financially supported by the National Natural Science Foundation of China (22174121, 22211530067, and T2250710180); the Natural Science Foundation of Guangdong Provincial Basic and Applied Basic Research Fund 2022 (Guangdong Hybribio); the Guangdong Pearl River Talent Program (2021CX02Y066); and the Shenzhen Bay Open Laboratory Fund 2021 by the Shenzhen Bay Laboratory, the CUHKSZ-Boyalife Joint Laboratory Fund, and the University Development Fund (UDF01002012).

Declaration of interests

The authors declare no competing interests.

Supplemental information

Supplemental information to this article can be found online at https://doi.org/10.1016/j.tibtech.2025.05.001.

References

1. Cohen, J.D. *et al.* (2018) Detection and localization of surgically resectable cancers with a multi-analyte blood test. *Science* 359, 926–930
2. Corman, V.M. *et al.* (2021) Comparison of seven commercial SARS-CoV-2 rapid point-of-care antigen tests: a single-centre laboratory evaluation study. *Lancet Microbe* 2, e311–e319
3. Peeling, R.W. *et al.* (2022) Diagnostics for COVID-19: moving from pandemic response to control. *Lancet* 399, 757–768
4. Klebes, A. *et al.* (2024) Emerging multianalyte biosensors for the simultaneous detection of protein and nucleic acid biomarkers. *Biosens. Bioelectron.* 244, 115800
5. Drain, P.K. *et al.* (2014) Diagnostic point-of-care tests in resource-limited settings. *Lancet Infect. Dis.* 14, 239–249
6. Gubala, V. *et al.* (2012) Point of care diagnostics: status and future. *Anal. Chem.* 84, 487–515
7. Liu, C. *et al.* (2021) Cytokines: from clinical significance to quantification. *Adv. Sci.* 8, 2004433
8. Falconnet, D. *et al.* (2015) Rapid, sensitive and real-time multiplexing platform for the analysis of protein and nucleic-acid biomarkers. *Anal. Chem.* 87, 1582–1589
9. Najjar, D. *et al.* (2022) A lab-on-a-chip for the concurrent electrochemical detection of SARS-CoV-2 RNA and anti-SARS-CoV-2 antibodies in saliva and plasma. *Nat. Biomed. Eng.* 6, 968–978
10. Zhou, J. *et al.* (2020) High-throughput single-EV liquid biopsy: rapid, simultaneous, and multiplexed detection of nucleic acids, proteins, and their combinations. *Sci. Adv.* 6, eabc1204
11. Klebes, A. *et al.* (2022) Multianalyte lateral flow immunoassay for simultaneous detection of protein-based inflammation biomarkers and pathogen DNA. *Sensors Actuators B Chem.* 355, 131283
12. Barletta, J.M. *et al.* (2004) Lowering the detection limits of HIV-1 viral load using real-time immuno-PCR for HIV-1 p24 antigen. *Am. J. Clin. Pathol.* 122, 20–27
13. Rissin, D.M. *et al.* (2010) Single-molecule enzyme-linked immunosorbent assay detects serum proteins at subfemtomolar concentrations. *Nat. Biotechnol.* 28, 595–599
14. Li, Y. *et al.* (2019) CRISPR/Cas systems towards next-generation biosensing. *Trends Biotechnol.* 37, 730–743
15. Dai, Y. *et al.* (2020) CRISPR mediated biosensing toward understanding cellular biology and point-of-care diagnosis. *Angew. Chem. Int. Ed.* 59, 20754–20766
16. Feng, W. *et al.* (2021) CRISPR technology incorporating amplification strategies: molecular assays for nucleic acids, proteins, and small molecules. *Chem. Sci.* 12, 4683–4698
17. Liang, M. *et al.* (2019) A CRISPR-Cas12a-derived biosensing platform for the highly sensitive detection of diverse small molecules. *Nat. Commun.* 10, 3672
18. Wu, Y. *et al.* (2022) A PAM-free CRISPR/Cas12a ultra-specific activation mode based on toehold-mediated strand displacement and branch migration. *Nucleic Acids Res.* 50, 11727–11737
19. Broto, M. *et al.* (2022) Nanozyme-catalysed CRISPR assay for preamplification-free detection of non-coding RNAs. *Nat. Nanotechnol.* 17, 1120–1126
20. Nguyen, L.T. *et al.* (2020) Enhancement of trans-cleavage activity of Cas12a with engineered crRNA enables amplified nucleic acid detection. *Nat. Commun.* 11, 4906
21. Aman, R. *et al.* (2020) Nucleic acid detection using CRISPR/Cas biosensing technologies. *ACS Synth. Biol.* 9, 1226–1233
22. Broughton, J.P. *et al.* (2020) CRISPR–Cas12-based detection of SARS-CoV-2. *Nat. Biotechnol.* 38, 870–874
23. Gootenberg, J.S. *et al.* (2017) Nucleic acid detection with CRISPR-Cas13a/C2c2. *Science* 356, 438–442
24. Guo, L. *et al.* (2020) SARS-CoV-2 detection with CRISPR diagnostics. *Cell Discov.* 6, 34
25. Chen, J.S. *et al.* (2018) CRISPR-Cas12a target binding unleashes indiscriminate single-stranded DNase activity. *Science* 360, 436–439
26. Kellner, M.J. *et al.* (2019) SHERLOCK: nucleic acid detection with CRISPR nucleases. *Nat. Protoc.* 14, 2986–3012
27. Ding, X. *et al.* (2021) Sensitive quantitative detection of SARS-CoV-2 in clinical samples using digital warm-start CRISPR assay. *Biosens. Bioelectron.* 184, 113218
28. Chen, Z. *et al.* (2021) CRISPR/Cas12a and immuno-RCA based electrochemical biosensor for detecting pathogenic bacteria. *J. Electroanal. Chem.* 901, 115755
29. Shi, K. *et al.* (2021) A CRISPR-Cas autocatalysis-driven feedback amplification network for supersensitive DNA diagnostics. *Sci. Adv.* 7, eabc7802
30. Deng, F. *et al.* (2024) Topological barrier to Cas12a activation by circular DNA nanostructures facilitates autocatalysis and transforms DNA/RNA sensing. *Nat. Commun.* 15, 1818
31. Li, S-Y. *et al.* (2018) CRISPR-Cas12a-assisted nucleic acid detection. *Cell Discov.* 4, 20
32. Pack, S.P. *et al.* (2010) Accurate guanine: cytosine discrimination in T4 DNA ligase-based single nucleotide polymorphism analysis using an oxanine-containing ligation fragment. *Anal. Biochem.* 398, 257–259
33. Conze, T. *et al.* (2009) Analysis of genes, transcripts, and proteins via DNA ligation. *Annu. Rev. Anal. Chem.* 2, 215–239
34. Barringer, K.J. *et al.* (1990) Blunt-end and single-strand ligations by *Escherichia coli* ligase: influence on an in vitro amplification scheme. *Gene* 89, 117–122
35. Zou, S. *et al.* (2024) CRISPR-Cas12a immunosensing on glass fiber for point-of-care quantification of multiple inflammation biomarkers in osteoarthritis. *Device* 2, 100319
36. Zhou, B. *et al.* (2021) SARS-CoV-2 spike D614G change enhances replication and transmission. *Nature* 592, 122–127
37. Harvey, W.T. *et al.* (2021) SARS-CoV-2 variants, spike mutations and immune escape. *Nat. Rev. Microbiol.* 19, 409–424
38. Jo, A. *et al.* (2023) Inaugurating High-throughput profiling of extracellular vesicles for earlier ovarian cancer detection. *Adv. Sci.* 10, 2301930
39. Blake, R. and Delcourt, S.G. (1996) Thermodynamic effects of formamide on DNA stability. *Nucleic Acids Res.* 24, 2095–2103
40. Weber, P.C. *et al.* (1989) Structural origins of high-affinity biotin binding to streptavidin. *Science* 243, 85–88
41. Paluzzi, V.E. *et al.* (2023) Near-quantitative preparation of short single-stranded DNA circles. *Angew. Chem. Int. Ed.* 62, e202218443
42. Sakhabutdinova, A. *et al.* (2017) Synthesis of circular DNA templates with T4 RNA ligase for rolling circle amplification. *Mol. Biol.* 51, 639–646

43. Gubu, A. *et al.* (2020) Synthesis and "DNA interlocks" formation of small circular oligodeoxynucleotides. *ACS Appl. Mater. Interfaces* 12, 12584–12590
44. Huang, Z. *et al.* (2022) Surface modification of liquid metal with p-aniline derivatives toward bioapplications: biosensing as an example. *ACS Appl. Mater. Interfaces* 14, 56429–56439
45. Diao, W. *et al.* (2024) EGaIn-modified ePADs for simultaneous detection of homocysteine and C-reactive protein in saliva toward early diagnosis of cardiovascular disease. *ACS Sensors* 9, 4265–4276
46. Jones, T.C. *et al.* (2021) Estimating infectiousness throughout SARS-CoV-2 infection course. *Science* 373, eabi5273
47. Li, D. *et al.* (2024) Isolation and quantification of L1CAM-positive extracellular vesicles on a chip as a potential biomarker for Parkinson's disease. *J. Extracell. Vesicles* 13, e12467
48. Kowal, J. *et al.* (2016) Proteomic comparison defines novel markers to characterize heterogeneous populations of extracellular vesicle subtypes. *Proc. Natl. Acad. Sci. U. S. A.* 113, E968–E977
49. Li, H. *et al.* (2024) Extracellular vesicular analysis of glypican 1 mRNA and protein for pancreatic cancer diagnosis and prognosis. *Adv. Sci.* 11, 2306373
50. Langelier, C. *et al.* (2018) Integrating host response and unbiased microbe detection for lower respiratory tract infection diagnosis in critically ill adults. *Proc. Natl. Acad. Sci. U. S. A.* 115, E12353–E12362
51. Cao, W. (2004) Recent developments in ligase-mediated amplification and detection. *Trends Biotechnol.* 22, 38–44
52. Wang, L. *et al.* (2019) 3′ Branch ligation: a novel method to ligate non-complementary DNA to recessed or internal 3′ OH ends in DNA or RNA. *DNA Res.* 26, 45–53
53. Kodidela, S. *et al.* (2018) Cytokine profiling of exosomes derived from the plasma of HIV-infected alcohol drinkers and cigarette smokers. *PLoS One* 13, e0201144
54. Van Niel, G. *et al.* (2018) Shedding light on the cell biology of extracellular vesicles. *Nat. Rev. Mol. Cell Biol.* 19, 213–228
55. Song, J. *et al.* (2024) Amplifying mutational profiling of extracellular vesicle mRNA with SCOPE. *Nat. Biotechnol.*, Published online October 7, 2024. https://doi.org/10.1038/s41587-024-02426-6
56. Huang, Y. *et al.* (2023) Toward a human brain extracellular vesicle atlas: characteristics of extracellular vesicles from different brain regions, including small RNA and protein profiles. *Interdiscip. Med.* 1, e20230016

STAR★METHODS

KEY RESOURCES TABLE

Reagent or resource	Source	Identifier
Enzymes		
EnGenLba Cas12a	New England Biolabs	M0653S
T4 DNA ligase	TaKaRa Bio	2011A
Exonuclease I	TaKaRa Bio	2650A
Exonuclease III	TaKaRa Bio	2170A
Antibody pairs and proteins		
Purified anti-human TNF-alpha	BioLegend	502802
Purified anti-human TNF-alpha	BioLegend	502901
Recombinant human TNF-α protein	Sino Biological	10602-HNAE
Recombinant Anti-IFN gamma Antibody	Sino Biological	11725-R238
Recombinant Anti-IFN gamma Antibody	Sino Biological	11725-R209
Recombinant human IFN-γ protein	Sino Biological	11725-R209
Recombinant Anti-IL-6 Antibody	Sino Biological	10395-MM02
Recombinant Anti-IL-6 Antibody	Sino Biological	10395-MM72
Recombinant human IL-6 protein	Sino Biological	10395-HNAH
Anti-CD81 monoclonal antibody	Proteintech	66866-1
Human IL-6 ELISA kit	Novus Biologicals	VAL102
Human IFN-γ ELISA kit	Novus Biologicals	VAL104C
Human TNF-α ELISA kit	Novus Biologicals	VAL105G
Chemicals, peptides, and recombinant proteins		
20 bp DNA Ladder (Dye Plus)	TaKaRa Bio	3420A
All oligonucleotides	Shanghai Sangon Biological Engineering Technology & Services Co. Ltd	Purification by high-performance liquid chromatography(HPLC)
Tris((1-benzyl-1H-1,2,3-triazol-4-yl) methyl) amine	Solarbio (Beijing, China)	YS157300
Tween-20	Sigma-Aldrich	P9416
MES	Sigma-Aldrich	M3671
EGaIn	Sigma-Aldrich	495425
Dynabeads MyOne Streptavidin C1 beads (Streptavidin-modified MBs)	Thermo Fisher scientific	65001
EDC	Thermo Fisher scientific	22980
sulfo-NHS	Thermo Fisher scientific	24510
4-Aminobenzoic acid	Aladdin	A108862
SYBR Green I	Aladdin	S171397
Taq pro-Universal SYBR qPCR Mix	Vazyme Biotech Co., Ltd. (Nanjing, China)	Q712-02
NHS Magnetic Beads Kit (2 μm average diameter)	Beaverbio Biotech Co., Ltd. (Suzhou, China)	70703
Streptavidin magnetic beads (300 nm average diameter)	Beaverbio Biotech Co., Ltd. (Suzhou, China)	22308
The SurePAGE™, Bis-Tris, 10x8, 4-12%, 10 wells	Genscript Biotech Co. Ltd (Nanjing, China)	M00652
The streptavidin conjugation kit	Abcam	ab102921
The streptavidin protein	Sigma-Aldrich	S4762

(continued on next page)

(continued)

Reagent or resource	Source	Identifier
bovine serum albumin (BSA)	Sigma-Aldrich	B2064
PDMS elastomers, including the silicone elastomer base and silicone elastomer curing agent	Dow Silicones	/
The glass optical fiber(diameter, 125 mm)	Ali-baba	G657-A2
Amicon Ultra-0.5 Centrifugal Filter Column -10 K and 30 K	Merck Millipore Ltd. (Billerica, MA).	(UFC501096) (UFC503096)
The pre-stained protein ladder	New Cell & Molecular Biotech Co., Ltd	P9006
Exosome panel (Calnexin, CD9, CD63, CD81, Hsp70, TSG101)	Abcam	ab275018
Ethanol, acetone, and sodium hydroxide	Xilong Scientific	/

EXPERIMENTAL MODEL AND STUDY PARTICIPANT DETAILS

The study was conducted at the Chinese University of Hong Kong, Shenzhen. All 56 eligible cervical tumor patients for this study accepted surgery and were followed up regularly. Patients provided written informed consent, and the study adhered to the principles outlined in the Declaration of Helsinki. Ethics approval (#B2023-112-01) was granted by the Institutional Research Ethics Committee of Sun Yat-sen University Cancer Center for the use of clinical specimens in research.

The Parkinson's disease detection study was approved by the Ethics Committee of Qilu Hospital, Shandong University, under ethics permission number KYLL-2023(ZM)-221. Written informed consent was also obtained from all participants. All 12 patients were recruited from Qilu Hospital of Shandong University in accordance with the ethics approval guidelines. Each participant was diagnosed with clinically established Parkinson's disease (PD) based on the International Parkinson and Movement Disorder Society (MDS) Clinical Diagnostic Criteria (cite). Individuals with a history of alcoholism, cancer, autoimmune disease, or acute/chronic inflammatory disorders were excluded from participation. Peripheral blood samples were collected in inert separation gel vacuum tubes, and serum samples were prepared by centrifugation at 3000 rpm for 5 min. The serum was then aliquoted in 100 µl per tube and stored at -80°C. Following serum preparation, EVs were isolated using CD81-functionalized magnetic beads (MBs), and the EV lysates were analyzed with the g-CURS system.

Probe information

The genomic information was acquired from the National Center for Biotechnology Information (NCBI, https://blast.ncbi.nlm.nih.gov/). The *Δ157-158* mutation sites in the *Delta* variant (OK411440.1) and *wild-type* (NC_045512.2, Gene ID: 43740568) of SARS-COV2 were selected as the study model. To assess the universality of the method, the representative infectious disease, HPV16 (NC_001526.4), and an interference agent, HPV18(NC_001357.1), were also assessed. The sequence alignment was processed by *SnapGene 6.0.2 (SnapGene Software)*. The free energy of the secondary structure of crRNA and sequences was calculated by the website (https://www.nupack.org/).

METHOD DETAILS

Ligation

The ligation reaction is carried out with 5 µM AP (5'-end segment with a phosphate modification, complementary and adjusted for each specific target, and a 3' tail with the determined ssDNA activator for CRISPR/Cas trigger), BP (complementary and tailored for each specific target, with a 5'-biotin modification), and 5 µM *Delta* target cDNA or alternative other-type cDNA. The ligation reaction is carried out in 1× T4 DNA ligase buffer (25 mM Tris-HCl, pH 7.6; 5 mM MgCl ; 0.5 mM ATP; 0.5 mM DTT; 2.5% w/v PEG-8000; Thermo Scientific) The mixture was pre-incubated the template with AP and BP at 95°C for 5 min, followed cooled to RT and addition of 100 U T4 DNA ligase to the reaction mixture and incubation at 37°C for varying durations, with intervals of 5 min. The same procedures were followed to characterize and optimize ligation procedures for HPV16 *E7* and HPV18 *E7*, as detailed in the Supplemental information. A 10-min ligation time was selected for subsequent reactions.

Verification of mutation tolerance of ssDNA activator

The free energy of the secondary structure of crRNA was calculated by the website (https://www.nupack.org/). The sequences were designed with different point mutations that occurred in the 5' end, 3' end, and the internal ssDNA activator. The verification proceeded with the reaction mixture, which contained 20 nM Cas12a RNP and 200 nM LR(TTATT) in 1× NEB buffer 2.1. The reaction was performed at 37°C, with kinetic data collected at 2-minute intervals. Fluorescence measurements were taken using an excitation wavelength of 485 nm and an emission wavelength of 535 nm.

Preparation of outer ssDNA circle of CRs

The CR was prepared utilizing the base stacking force-assisted method, designed by Victoria etc [41]. In short, the dumbbell structure Hc (20 μM), an equal molar concentration of Lc (20 μM), and 500 U T4 ligase were mixed thoroughly in the 1x T4 ligase buffer to a 50 μL reaction volume, which was incubated at room temperature for 16 h ligation. After the inactivation of T4 ligase at 95 °C for 5 min, the ligation mixture was incubated with 25 U exonuclease III and 12.5 U exonuclease I in exonuclease I buffer with a 100 μL reaction volume reacted at 37 °C for 3.5 h to remove the remaining Lc completely. The purified products were subsequently loaded into the 10K Amicon Ultra column with the centrifugation at 1,4000 g for 10 min (Eppendorf centrifuge 5424R) to remove the possible polymeric circle products (the by-products were intercepted in the upper layer of the column because of their large molecular mass). The sublayer solution containing the purified monomeric circle was stored at -20°C for several days before use.

The efficiency of forming the small-sized ssDNA circle by two additional methods (Sc-assisted-, and click chemistry-assisted-circle formation) were compared. As for the Sc-assisted approach, the other ligation reaction conditions and reactants were exactly the same as the Hc-assisted one, except that an equal amount of Sc replaces Hc for the reaction (20 μM Sc, 20 μM Lc and 500 U T4 ligase in the 1 x T4 ligase buffer, react at RT for 16 hr). For the click chemistry-assisted method, as described in Deng and coworkers. [30], the linear circle sequences (L-outer1 or L-outer2) were modified with the biotin group in the middle for SA conjugation, azide (N3) at the 5'-end, and 3'-CHCH at the 3'-end for Cu+/TABA-catalyzed click chemistry. The preparation of magnetic beads involved blocking 0.4 ml of 0.5% w/v streptavidin-modified magnetic beads (300 nm) with 1% Bovine Serum Albumin (BSA) for 1 h. These beads were then incubated with 1 ml of 0.5 μM biotinylated linear-ssDNA for 1 h, followed by washing with 1x wash buffer C to remove any unbound linear-ssDNA. The beads were subsequently treated with a click chemistry reaction mixture (1.0 mM CuSO , 2.0 mM TCEP, and 100 μM TBTA) and incubated for 12 h at room temperature. Following synthesis, excess reagents were removed by washing with 1x wash buffer C. To degrade any residual linear-ssDNA, 100 U of Exonuclease I was added, and the mixture was incubated at 37°C for 30 min. A final purification with 1x wash buffer C was performed 3 times, and the product was released from the beads in the 1 x TE buffer by heating at 95°C for 30 min. The supernatant was collected for subsequent dPAGE analysis.

Yield estimation of ssDNA monomeric circles

A standard curve was established to quantify the circles by serially diluting Lc with a 10-fold factor, staining with SYBR Green I, and measuring the fluorescence signal. The concentration of staining purified circles was then determined using the standard curve instead of using a Microvolume UV Spectrophotometer. This process facilitated the evaluation of the yield, which was determined using the formula: Yield (%) = (Purified product concentration × final volume) / (Starting sequence concentration × volume) × 100%. To form CRs, incubate the ssDNA outer circle with an equimolar concentration of inner circle sequences at 95°C for 5 min. Keep the CRs at 4°C for subsequent experiments.

Characterization of ssDNA monomeric circles

The ssDNA monomeric circle was characterized by the dPAGE. A 15% denaturing PAGE gel was prepared using a 30% 29:1 acrylamide/bisacrylamide solution, 7 M urea, and TBE buffer containing 89 mM tris base (pH 8.0), 89 mM boric acid, and 2 mM EDTA. The gel was pre-run at 150 V and 50°C for 30 minutes. Simultaneously, ligation samples and reference sequences (5 μL 20 bp DNA ladder, 10 μL 5 μM Sc, Lc, Hc, separately, and 10 μL ligation products) were incubated with an equal volume of pure formamide at 95°C for 25 minutes to denature their secondary structure. The samples were then loaded and run at 100 V and 50°C for 1.5 hours until the second band of the loading buffer reached the bottom of the gel (Bio-Rad, Mini-PROTEAN Tetra system). Gel staining proceeded with 1x SYBR Green I for 20 minutes at room temperature with gentle rotation, and the results were scanned using the Molecular Imager system (Bio-Rad, ChemiDoc XRS+).

The NuPAGE characterized the intermediate products of the CR. The 10% native PAGE gel was prepared with 30% 29:1 acrylamide/bisacrylamide solution and TAE/20 mM Mg^{2+} buffer containing 40 mM tris base (pH 8.0), 20 mM acetic acid, 2 mM ethylenediaminetetraacetic acid (EDTA) and 24 mM magnesium acetate. Samples containing10 μL 5 μM (Sc, Lc, Hc, Sc-Lc mixture, and Hc-Lc mixture) were mixed thoroughly in 1x TAE/20 mM Mg^{2+} buffer at RT. The gel was run at 4 °C at 220 V, followed by staining with 1x Sybr Green I, and finally scanned by the Molecular Imager system.

Verification of amplification capability of CRs in homogeneous solution

The signal amplification capability of CR-assisted CRISPR/Cas12a using the ssDNA activator as the template for identifying nucleic acid targets at low concentrations was studied. As a control, a LR (TTATT) was employed. Cas12a cleavage efficiency for two types of reporter was initiated with 1 nM ssDNA activator. The reaction mixture contained 20 nM Cas12a RNP and 200 nM reporter (linear or circular) in 1× NEB buffer 2.1. The reaction was performed at 37°C, with kinetic data collected at 2-minute intervals. Fluorescence measurements were taken using an excitation wavelength of 485 nm and an emission wavelength of 535 nm, recorded using the SpectraMax ID5 multimode microplate reader (Molecular Devices, USA).

The signal-to-noise ratio was measured and compared across serially diluted ssDNA activators ranging from 1 nM to 1 aM using a 10-fold dilution factor. The reaction mixture contained 20 nM Cas12a RNP, 1x NEBuffer r2.1, and 200 nM LR or CR. The enzyme cyclic reaction produced a 30-minute endpoint fluorescence signal at 37°C.

Modification and characterization of glass fibers

The fabrication of the biosensing interface was modified following a protocol similar to a previously described procedure [35,44]. Specifically, EGaIn-PABA nanoparticles were synthesized by mixing 13 μl of EGaIn (62.5 mg) with 1 ml of 0.5 M HCl for 2 hours, followed by centrifugation at 10,000 rpm for 3 min (Eppendorf 5424R centrifuge) and washing with ethanol. The EGaIn was then dispersed in 5 ml ethanol containing 10 mM PABA, sonicated at 4°C for 2 h with 20 kHz ultrasonic power, and excess PABA in the supernatant was removed by centrifugation at 10,000 rpm for 10 min. The final EGaIn-PABA product was stored at 4°C and characterized by dynamic light scattering and zeta potential analysis (Malvern Panalytical, UK). For the biosensing interface fabrication, a glass fiber (125 μm core) was stripped, cleaned by a 30-min immersion in acetone, and subsequently treated with piranha solution for 1 hour and exposed to plasma (100 W) for 30 s (PR301, Yamato Scientific, Japan) to introduce hydroxyl groups. After surface amination with 2% (v/v) APTES ethanol solution, the fibers were incubated with EGaIn-PABA nanoparticles at room temperature overnight under 30 W ultrasonication. The EGaIn-PABA-fibers were then activated with 50 mM EDC and 200 mM sulfo-NHS in 0.1 M MES buffer (pH 6) for 30 min at room temperature and immobilized capture antibodies (25 mg/ml) or streptavidin (50 mg/ml) at 4°C overnight. Finally, the functionalized fiber was blocked with 5% (w/v) BSA at 4°C for 1 h, rinsed with water, and dried under nitrogen.

Optimization of formamide concentration in wash buffer F

The purification process of the SA-fiber to capture ligation products involves using wash buffer F with varying formamide concentrations (0–40%, v/v) to minimize nonspecific primer coupling caused by hydrogen bonding. The ligation reaction mixture, comprising 100 pM synthetic HPV16 *E7* cDNA segment, 1 μM AP16, 1 μM BP16, and 100 U T4 ligase in 1× T4 ligation buffer, was incubated at 37°C for 10 minutes, followed by enzyme inactivation at 95°C for 5 minutes, and the resulting ligation products were incubated with SA-fiber at room temperature for 15 minutes. For the amplification reaction, a mixture containing 20 nM Cas12a RNP and 200 nM CR in 1× NEB buffer 2.1 was incubated at 37°C for 15 minutes, followed by signal readout by SpectraMax ID5 (Molecular Devices, USA).

Preparation of dAb-ssDNA conjugation

The preparation of dAb-ssDNA conjugation proceeded according to the protocol advised by commercial kits (Abcam limited). In summary, 10 μL of 1 mg/ml antibodies were gently mixed with 1 μL of modifier reagent for 10 min. Subsequently, the mixture was used to resuspend 10 mg of lyophilized streptavidin by gently pipetting up and down and then left standing for 3 h in the dark at room temperature. Following this, 1 μL of quencher reagent was added to the mixture and gently mixed for 30 min. Afterwards, the resulting 10 μg streptavidin-labeled dAb was incubated with 10 μL of 100 mM biotinylated trigger ssDNA at 4 °C overnight. The conjugate was then further purified using a centrifugal filter unit (Merck Millipore, 30 kDa) and dissolved in 100 μL of 1x PBS solution. The final detection conjugate was stored at 4 °C for the following usage.

Preparation of g-CURS for nucleic acid detection

In our proposed method, the subsequent signal amplification depended on the connection of the designed AP and BP by T4 DNA ligase, ensuring the high specificity of the assay. In the presence of target cDNA(*Delta* or HPV16 *E7*), subsequent reactions in the ligation system (10 μL) were prepared by mixing 1 μM AP and 1 μM BP in 1x T4 ligation reaction buffer. The reagent mixture was then preheated at 95°C for 5 min to ensure proper matching and complementation. After cooling down to room temperature, 100 U T4 ligase was added to the mixture for ligation and reacted at 37 °C for 10 min. The SA-modified glass fiber was incubated in the ligation mixture to capture the ligation products for 15 min. To remove nonspecific probes, the ligation product-functionalized fiber was immersed in 1x wash buffer F at 37°C for 5 min, followed by two rinses with 1x wash buffer C to eliminate residual formamide. The product-conjugated glass fiber was then immersed in the CRISPR/Cas12a reagent (20 nM Cas12a RNP, 1x NEBuffer r2.1, 200 nM CR, premixed at 4°C), initiating the cascade amplification reaction to produce a fluorescence signal at 37°C for 15 min. Endpoint fluorescence was measured using the SpectraMax ID5 multimode microplate reader (Molecular Devices, USA) with excitation at 585 nm and emission at 635 nm.

Preparation of g-CURS for protein detection

The capture antibody-modified sensing interface on the glass fiber was incubated in the target analyte solution for 30 min at RT, followed by exposure to the dAb-ssDNA conjugate (dilution ratio 1:100, concentration 1 mg/ml) to facilitate the formation of a sandwich immunoassay. The incubation time with dAb-ssDNA was limited to 30 min to prevent nonspecific adsorption. After each incubation with different steps, wash with 1 x PBST to remove excess reagents and nonspecific adsorption. The g-CURS assay, consisting of the 20 nM Cas12a RNP, 1x NEBuffer r2.1, 200 nM CR, premixed at 4°C. After immersing the immunoassay-conjugated glass fiber in the reaction reagent, the ssDNA-modified dAb of the sandwich immunosensor on the glass fiber activated the CR-assisted CRISPR/Cas12a assay, initiating exponential signal accumulation at 37°C. The 15-min endpoint fluorescence signal was measured using the SpectraMax ID5 multimode microplate reader (Molecular Devices, USA) with excitation at 585 nm and emission at 635 nm.

Preparation of the detection chip in the portable device

The chip preparation for the portable detection device followed a protocol similar to that developed by Zou and coworkers [35]. In brief, a chip was fabricated on a PDMS substrate with a 3D-printed mold. The chip features five individual semi-cylindrical shape channels (30 mm in length, 2 mm in diameter, 50 μL liquid volume). The molds were printed using a microscale 3D printer (nanoArch S140, BMF Material Technology, China) and rinsed with isopropanol for 10 min to avoid PDMS curing. The PDMS prepolymer was mixed with a curing agent in a 10:1 weight ratio, poured into the 3D-printed molds, and cured for 30 min at 80°C. To ensure strong adhesion between the PDMS layer and glass slides, both surfaces were treated with oxygen plasma at 100 W for 30 s, immediately bonded, and heated the assembled chips at 80°C for 30 min to strengthen the bond further. Finally, a 25 μL CRISPR/Cas12a mixture was injected into each channel, which was then sealed and stored at 4°C until needed. The CR assisted-CRISPR/Cas12a reaction is activated only when the corresponding glass fiber sensors are inserted into the channels.

Validation of HPV16 E7 mRNA in cervical tumor clinical samples by RT-PCR

The total mRNAs were first extracted from a cohort of 56 cervical tumor tissue samples using TRIzol (Life Technologies). After resuspending the mRNA pellet in DEPC-treated water, the first strand of cDNA was synthesized according to the manufacturer's instructions using the Color Reverse Transcription Kit (EZB, A0010CGQ). RT-PCR assays were then performed on the real-time PCR system (Thermo Fisher Scientific, applied biosystems, QuantStudio 3), which was used for thermocycling and fluorescence detection. RT-PCR amplification for HPV16 *E7* cDNA was conducted in a total volume of 20 μl, consisting of 10 μl of 2× qPCR mix, 2 μl each of forward and reverse primers (1 μM), 1 μl of cDNA, and distilled water to reach a final volume of 20 μl per sample. The RT-PCR procedure consisted of a hold stage at 95°C for 30 s, followed by a PCR stage repeated for 40 cycles, with the following procedure: 95°C for 10 s, 62°C for 30 s, and 72°C for 20 s. The cycle threshold (Ct) value represented the relative cDNA level during amplification. A Ct value was considered significant (positive) if it was at least six cycles lower than the control Ct value.

Validation of HPV16 E7 mRNA in cervical tumor clinical sample by the g-CURS system

A sample volume of 1 μl was used in the g-CURS system to ensure consistency with RT PCR. A cohort of 56 clinical samples was analyzed using the g-CURS system. The reaction mixture included 20 nM Cas12a RNP, 1x NEBuffer r2.1, and 200 nM CR, premixed at 4°C. The endpoint fluorescence signal was measured after 15 min using the SpectraMax ID5 multimode microplate reader. To

accommodate a POCT scenario, 20 representative clinical samples were analyzed using a portable device equipped with a 37 °C heating module. To adapt the system for the portable device, the fluorophore (Texas Red) was replaced with FAM, and the CR concentration was adjusted to 400 nM.

Preparation and characterization of EVs from PD serum samples

The preparation of anti-CD81-conjugated MBs was based on procedures developed by Li and coworkers [47]. Then, the anti-CD81-conjugated MBs (200 µl, 10 mg/ml) were mixed with 1 ml diluted serum samples for incubation overnight at 4 °C to isolate the EVs. The MBs-EVs conjugates were enriched by a magnetic stand and washed with PBST. After removing the supernatant by a magnet, 60 µl of lysis buffer was added to the mixture shaking at RT. And lysate was stored at 4 °C for subsequent protein detection. EVs eluted from anti-CD81-conjugated MBs were prepared for nanoparticle tracking analysis (NTA) (NanoSight NS300 (Malvern Panalytical, UK)) by adding 20 µl of glycine solution (8 mM, pH 2.9) to the MB-EV conjugates, followed by gentle shaking at 200 rpm for 10 minutes. The pH was then adjusted to neutral using 20 µl of 1 M Tris solution (pH 9.5). NTA was employed to measure EV concentration by tracking the particles' Brownian motion, with the Stokes-Einstein equation applied to calculate their diameter and concentration. For protein analysis in WB (electrophoresis instrument,1658001, Bio-Rad Laboratories, USA) analysis, EVs were lysed in 15 µl 4% (w/w) LDS solution and diluted with 15 µL 4% (w/w) SDS loading buffer with a gentle shaking at 200 rpm for 30 s. After heating at 95°C for 10 minutes, the protein-containing supernatant was collected using a magnetic stand. WB analysis was then performed to detect syntenin-1, CD9, CD63, and HSP70, aiding in the characterization of EVs.

Validation of g-CURS-assisted protein detection in EV lysates

The EV lysates were diluted 10-fold for ELISA analysis of IL-6, TNF-α, and IFN-γ. Cytokine concentrations were measured according to the manufacturer's instructions. For clinical analysis of small-volume samples using the g-CURS system, the EV lysates were diluted with 1x PBS at the same ratio, resulting in a total volume of 50 µl for multiplex cytokine detection (5 µl EV lysate in 45µl 1 xPBS). Three different capture antibody-modified glass fibers (IL-6, TNF-α, and IFN-γ) were simultaneously incubated with the diluted sample solution for 30 minutes at RT to capture the corresponding target proteins. This was followed by exposure to a 50 µl mixture of dAb-ssDNA conjugates (1:100 dilution ratio), consisting of three distinct dAb-ssDNA conjugates, to facilitate the formation of a sandwich immunoassay. A fourth fiber, unmodified with any capture antibodies, served as a blank control. The incubation with dAb-ssDNA conjugates was limited to 30 min. The endpoint fluorescent signal was collected from individual fibers after inserting them into their respective reaction component, including 20 nM Cas12a RNP, 1x NEBuffer r2.1, and 200 nM CR, and heated at 37°C for 15 min. We tested a cohort of 12 EV lysate samples obtained from Qilu Hospital, Shandong University, under approved ethical guidelines to assess the potential clinical application.

QUANTIFICATION AND STATISTICAL ANALYSIS

Statistical analyses were conducted in GraphPad Prism version 10.2.3 (GraphPad Software). The figures were processed and integrated by Adobe Illustrator 2021 (Adobe Illustrator Software). For normal distributions, the differences between the two groups were evaluated using a t-test, and the significance level was set as $P < 0.05$ (* $P < 0.05$, ** $P < 0.01$, *** $P < 0.001$, and **** $P < 0.0001$). Differences between group levels were analyzed with a two-way analysis of variance (ANOVA). All data are displayed as mean ± standard deviation (SD). Determining the LoD involves systematically diluting the antigen or nucleic acid concentration using gradient dilution techniques. LoD is defined as the minimal practical dilution concentration.